2017

Stream restoration effects on hydraulic exchange, storage and alluvial aquifer discharge

Christine M. Brissette
University of Montana, Missoula

STREAM RESTORATION EFFECTS ON HYDRAULIC EXCHANGE, STORAGE AND ALLUVIAL AQUIFER DISCHARGE

By

CHRISTINE MARIE BRISSETTE

Bachelor of Science, University of Vermont, Burlington, Vermont, 2008

Thesis

presented in partial fulfillment of the requirements for the degree of

Master of Science in Forestry

The University of Montana Missoula, MT

Official Graduation Date May 2016

Approved by:

Scott Whittenburg, Dean of The Graduate School Graduate School

Dr. Kelsey Jencso, Chair Department of Forest Management

Dr. W. Payton Gardner, Co-Chair Department of Geosciences

Dr. Lisa Eby Department of Ecosystem and Conservation Sciences

Dr. H. Maurice Valett Division of Biological Sciences

Brissette, Christine, M.S., Spring 2016 **Forestry**

Stream restoration effects on hydraulic exchange, storage and alluvial aquifer discharge

Chair: Dr. Kelsey Jencso

Co-Chair: Dr. W. Payton Gardner

Stream restoration is increasingly being considered as a climate change mitigation tool, altering the storage and exchange capacities of streams and their adjacent alluvial aquifers. While previous research has shown that added geomorphic complexity and increased width-to-depth ratios can enhance hydraulic exchange and alluvial aquifer storage, few studies have used field data to link these changes in form to baseflow generation. In this paper, we quantify the effect of stream restoration on nested scales of hydraulic exchange and temporal patterns of alluvial aquifer recharge and discharge. Our work compares a restored and degraded reach on Ninemile Creek, Montana following extensive placer mining in the late 1800's. Using a combination of topographic and morphologic surveys, well transects, piezometers and tracers, we monitored hydraulic exchange processes across multiple spatial scales and six flow stages. We then used ^{222}Radon and synoptic discharge measurements to evaluate reach-scale alluvial aquifer recharge and discharge over the 2016 hydrograph recession. We found that changes in channel form increased transient storage and induced feature-scale vertical exchange not observed in the degraded reach. However, vertical exchange flux and depth in the restored reach were limited by reduced subsurface hydraulic conductivity. Lateral gradients showed increased alluvial aquifer recharge and underflow in the restored reach, in contrast to persistent alluvial aquifer drainage seen in the degraded reach. The cumulative impact of restoration resulted in a longer period of alluvial aquifer recharge early in the season, and higher volumetric discharge at baseflow. Our results support the theory that restoration can increase storage and baseflow discharge, while emphasizing that site-specific influences can outweigh the intended effects of restoration. This work is a critical step towards understanding the efficacy of restoration in improving late season flows in the context of a changing climate and increased demand for water resources.

1. INTRODUCTION

The effect of stream restoration on hydraulic exchange and baseflow generation is poorly quantified. However, stream restoration is increasingly being considered as a climate change mitigation tool to improve the adaptability and resiliency of aquatic resources. One of the most emphasized climate change predictions for Western U.S. snow-dominated watersheds is the forecasted shift in spring snowmelt timing, resulting in earlier, more variable runoff (Barnett et al. 2005; Green et al. 2011; Huntington and Niswonger, 2012; IPCC, 2014). This shift will likely have profound effects on groundwater recharge-discharge dynamics, with earlier drainage of alluvial aquifer reservoirs, resulting in reduced storage and amplified water shortages in mid-to-late-summer (Barnett et al., 2008; Huntington and Niswonger, 2012). Trends in this region, in fact, already show patterns of reduced summer flows (Kim and Jain, 2010; Moore et al. 2007) with the most dramatic reductions occurring in the driest years (Luce and Holden, 2009).

In reaction to these challenges, there is a growing interest across academic, policy and management communities to explore stream restoration techniques that can promote natural water storage. These techniques physically manipulate channel and floodplain form to increase volumetric storage capacity of the shallow alluvial aquifer and alter the hydraulic exchange processes that affect retention and discharge within storage zones. While many studies have linked channel geomorphic form to individual hydraulic exchange processes (e.g. hyporheic exchange or transient storage), few evaluate the net impact of multiple forms of exchange, nor their influence on seasonal trends of alluvial aquifer recharge and discharge. Furthermore, little research has evaluated the efficacy of restoration for increasing volumetric base flow discharge outside of modeling frameworks. In their review of "River corridor science," Harvey and Gooseff (2015) emphasize the challenge of - and need for - research linking small-scale mechanistic drivers of hydrologic exchange with large-scale fluvial and ecologic responses. Here, we quantify the effect of restoration on nested paths of hydraulic exchange and temporal patterns of alluvial aquifer recharge and discharge.

In the last half century, our conceptual model of streams has shifted from "pipe-like" channels to dynamic systems of surface and subsurface exchange (e.g. Bencala et al, 2011; EPA, 2015; Hauer et al. 2016; Harvey & Gooseff, 2015; Stanford & Ward, 1993). Streams gain and lose water across a range of spatial scales, from centimeters in the near-bed hyporheic zone, to kilometers across groundwater systems and from upland environments. Our research focuses on the river corridor (sensu Harvey and Gooseff, 2015), encompassing both the channel and the alluvial

aquifer adjacent to, and beneath the stream. This is the area through which vertical, lateral and down-gradient hydrologic transport occurs, connecting the stream, groundwater, and hillslope hydrologic systems. Bidirectional exchange between these systems is often referred to as "hydrologic connectivity," with high levels of connectivity associated with ecosystem buffering (EPA, 2015; Harvey and Gooseff, 2015; Hauer et al. 2016; Jencso et al., 2010; Standford & Ward, 1993). Human impacts on the landscape such as mining, roads and development can, therefore, disrupt natural patterns of hydraulic exchange and inhibit the physical and biotic processes that rely on hydrologic connections (Kasahara et al. 2009; Kondolf et al., 2006). In turn, restoration can alter, reinstate or amplify desired flowpaths and their associated hydrological and ecosystem functions.

Hydraulic exchange forms an essential connection between terrestrial, subterranean and aquatic systems. Flowpath length and residence time in the subsurface exert a primary control over many chemical (Hill et al.,1996; Puckett et al., 2008; Valett et al., 1997), thermal (Arrigoni et al., 2008; Brunke and Gosner, 1997) and fluvial (Cardenas 2007; Helton et al., 2014; Payn et al 2012) processes. Flow paths through the river corridor often follow a nested, hierarchical pattern, with exchange initiated by variability in channel and floodplain topography (Berkowitz et al. 2006; Cardenas 2007; Gooseff et al. 2006; Poole et al., 2008; Stonedahl et al. 2010). The scale of the feature inducing exchange (wavelength and amplitude) positively correlates with the depth and residence time of subsurface flow (Marzadri et al., 2014; Stonedahl et al. 2010; Tonina & Buffington 2011). This results in residence times that often follow a power-law distribution, with numerous short-scale, rapid flow paths contained within increasingly larger-scale, longer-duration subsurface flows (Cardenas, 2007; Cardenas, 2008; Poole et al., 2008). Recent work has also shown that that these nested flow paths are highly influential on one another (Stonedahl et al. 2010) and therefore cannot be studied in isolation.

The length and residence time of exchange is dictated by the physical environment water moves through. Our work evaluates three scales of exchange: *1) Transient storage*, representing the non-advective portion of in-stream flow often associated with eddies and short-term hyporheic exchange. Transient storage increases with channel sinuosity (Patil et al., 2013; Gooseff et al. 2007), bed roughness (Gooseff et al. 2007; Wondzell, 2006) woody debris (Harvey et al., 2003; Salehin et al., 2003) and decreased channel slope (Patil et al., 2013; Gooseff et al. 2007) *2)Vertical hydraulic exchange* that is driven by pressure gradients created by channel topography (e.g. bed roughness, riffles) and modulated by the hydraulic conductivity of the substrate,

regulating subsurface velocities and creating tortuous, preferential flow paths in heterogeneous substrates (Harvey and Bencala, 1993; Tonina and Buffington, 2009; Tonina et al. 2016; Woessner, 2000); and *3) Lateral to down-valley flow*, driven by the relative elevations of the stream and water table (Woessner 2000) and strongly impacted by basin and aquifer characteristics such as valley slope, hydraulic conductivity, aquifer size (Larkin and Sharp, 1992; Woesser, 2000) and the degree of hydrologic connectivity with uplands environments (Jencso et al 2010; Payn et al. 2012).

Cumulatively, the combination of nested exchange processes can have significant influence on temporal patterns of alluvial aquifer recharge and discharge. Alluvial aquifers can be filled and drained through several mechanisms. First, longer hydraulic exchange flowpaths inherently result in longer subsurface residence times. Water leaving the stream and entering the subsurface is slowed by its interaction with the substrate and can be drawn away from the stream towards areas of lower hydraulic potential in the alluvial aquifer. Bank storage, for example, is a well-documented process (Todd, 1956; Whiting and Pomeranets, 1997) that occurs when stream stage exceeds the water table height (usually during Spring snowmelt in the Rocky Mountains), creating a gradient away from the stream that recharges the alluvial aquifer. As stream stage recedes, this gradient reverses, supporting streamflow. Inflows from hydrologically connected hillslopes are also a major source of alluvial water, as saturated flow from steep, upslope positions moves towards lower gradient valleys. Finally, groundwater discharges into the alluvial aquifer from deeper, broader aquifer sources. These three processes jointly fill the alluvial aquifer, which functionally "stores" water until it is discharged as streamflow down-gradient minutes, hours, days, months or years later (Cardenas, 2007; Helton et al. 2014) . The residence time of water in the aquifer, and the duration of the recharge and discharge period is highly influenced by the relative elevations of the stream and groundwater (Schilling et al. 2006; Woessner, 2000; Whiting and Pomeranets, 1997), the volume of the alluvial aquifer (Hammersmark et al. 2008; Jensco et al, 2010; Whiting and Pomeranets, 1997), and the hydraulic conductivity of the substrate (Whiting and Pomeranets, 1997; Woessner, 2000). While stream restoration has little impact on upslope and broad aquifer characteristics, it can substantially alter valley and channel form, and thus surface and alluvial aquifer exchange. Incised channels, for example, have a stronger lateral flow component (Larkin and Sharp, 1992), resulting in a narrower spatial zone of influence, shorter bank storage period and rapid drainage of stored alluvial water (Schilling et al. 2004, 2006). Reducing channel incision reduces overall gradients between the stream and alluvial groundwater system, and can result in a stronger down-valley

underflow component (Larkin and Sharp, 1992), longer duration of aquifer recharge and a prolonged release of stored water, shortening the base flow period (Hammersmark et al., 2008).

Our research evaluates a common stream restoration approach that simultaneously impacts multiple scales of exchange, and thus temporal trends water storage and discharge dynamics (Appendix A, Figure 1). This approach includes 1) Increasing the complexity of stream bed elevations to enhance vertical exchange; 2) Increasing sinuosity to activate transient storage zones and enhance exchange through banks and bars; and 3) Raising the channel bed elevation to neutralize the lateral gradient, promoting a longer bank storage storage period, a prolonged release of stored water and increased volumetric discharge at low flows. Using a combination of wells, piezometers, discharge measurements and groundwater tracers, we quantified the effects of restoration on nested sales of exchange and the resulting temporal patterns of alluvial aquifer recharge and discharge.

2. STUDY AREA

2.1. Climate, Soils and Lithology

Ninemile Creek is a tributary to the Middle Clark Fork River in Northwest Montana, USA (Appendix A, Figure 2a). The research site is located approximately 30 km upstream from the Clark Fork River confluence at approximately 1200 meters elevation. The basin contributing area from the downstream-most point of the study area is 60.5 km^2 and is primarily coniferous forest, managed by Lolo National Forest.

Watersheds in this region are snowmelt-dominated, with peak discharge occurring in May-June. Following snowmelt, the hydrograph recedes towards a base flow period in August-September with small increases in flow that are associated with fall precipitation in the form of rain and snow. Discharge at the project site ranged from approximately 100-900 liters sec^{-1} in 2016. There are no perennial surface flows into the study area, though small ephemeral return flows occur at the break in slope between the valley and convergent uplands during snowmelt runoff.

The Precambrian Belt Supergroup comprises the underlying lithology of the Ninemile basin. The lithology is dominated by the Missoula Group of the Belt Supergroup consisting of metasedimentary argillites, quartzites, and limestones. Valley alluvium is composed of weathered Belt, tertiary colluvial sediments and glacial lacustrine deposits from Glacial Lake Missoula. The river flows down the strike of the Ninemile fault, a regional normal fault, which was likely the

source of gold deposits extracted from the region.

2.2 Mining and Restoration History

Gold placer deposits were discovered in the late 1800's and were mined through the 1950's primarily via dry-land dredging. This resulted in a straightened, incised channel (Appendix A, Figure 2c) with 10-meter tall overburden piles and dredge ponds throughout the floodplain extent. In 2014, Trout Unlimited initiated restoration of the Ninemile Creek, removing overburden piles, filling dredge ponds and establishing a new, single-thread meandering stream channel (Appendix A, Figure 2c) with adjacent floodplain wetlands. Restoration designs included raising the channel bed elevation to increase lateral connectivity between the stream and floodplain and adding sinuosity and riffle-pool sequences (typical of a Pool-Riffle channel sensu Montgomery and Buffington,1997). The new channel was constructed using sorted alluvial fill from the project site.

This research compares a portion of the 2014 restoration site (351 m reach length) to a , downstream reach still in post-mining condition (224 m reach length, with a 200-meter break between reaches) (Appendix A, Figures 2b-d). The valley and floodplain width through the project area (disregarding channel incision) are approximately 125 meters and 35 meters wide respectively, with a valley slope of 0.015. One important anomalous feature in the degraded reach is a channel-spanning beaver dam approximately 80 meters from the top of the reach.

3.0 METHODS

3.1 Sampling Design

We selected the restored and degraded reaches based upon restoration-induced differences in topographic and morphologic characteristics known to influence surface and subsurface water movement. These included channel width-to-depth ratios, slope, sinuosity and bedform complexity. A review of geologic maps (Natural Resource Conservation Services), aerial imagery (Google Earth, 2016) and mining records (Montana Bureau of Mines and Geology) indicated that the restored and degraded reaches were analogous in terms of their soils, geology, upslope topography and basin land cover. Valley slope and valley width were also consistent among the restored and degraded reaches. The hillslope area contributing to the restored and degraded reaches were 0.54 km^2 and 0.33 km^2 respectively. Field observations and conversations with restoration project managers confirmed that the selected sites offered a viable comparison of the

impact of restoration.

Each of the stream reaches was instrumented in March and April 2016. Appendix A, Figures 2c and 2d illustrate the locations of well transects and piezometers. We equipped shallow groundwater wells and stilling wells with pressure transducers (Solinst 3001 Levelogger Junior Edge M10, Georgetown, ON, Canada) to measure hourly groundwater and stream heights from April – November 2016. We also completed synoptic surveys of piezometers and discharge, and collected water samples for ^{222}Radon analysis six times from May 24-November 11, 2016, with the goal of evenly characterizing the hydrograph recession.

3.2 Hydrometeorology

Precipitation and snowmelt data were collected from the nearest USDA SNOTEL site, Sleeping Woman (#783) at 1875 m. elevation. This site is 600 meters above and 25 km. east-southeast of the project area, with similar characteristics to the upper basin that drains towards Ninemile Creek. These data were included in our analysis to represent the timing (not magnitude) of precipitation events in the area and to evaluate the seasonal snowmelt trends that contributed to hydrologic responses measured at our project site.

3.3 Characterization of channel and floodplain topography and geomorphology

We conducted geomorphic and topographic surveys to quantify differences in the physical form of the channel and floodplain in restored and degraded reaches. Using a total station, we surveyed the longitudinal profiles of each reach (approximately 1-meter resolution), and interpolated a 10 cm resolution spline to that profile for more detailed feature analyses. We also surveyed cross-sections (9 in degraded and 10 in restored) to calculate width-to-depth ratios. Survey points were georeferenced and transformed using benchmark points collected with a high resolution GPS unit (Trimble Nomad with GPS Pathfinder ProXRT receiver, Trimble Navigation Limited, Westminster, CO, USA). From these survey data, we calculated average streambed slope (upstream riffle to downstream riffle), bankfull stage, width-to-depth ratios and sinuosity (valley length/stream length). We described streambed topographic complexity by calculating thalweg variation, following the methods of Walters et al. (2003). We fit a linear regression to the longitudinal profile using the upstream and downstream-most elevations. Large residuals around the trendline correspond to prominent bed features, so a lower r^2 value and larger standard deviation of residuals indicate more complex streambed topography.

To characterize grain size distributions of the streambed, we used a modified Wolman Pebble

Count (Wolman, 1954). Bed surface textural patches were visually assessed and mapped to estimate percent cover of each patch, and transect locations for pebble counts were stratified based on these textural patches. In the degraded reach, we identified 3 textural patches, with 105-172 total grains measured per patch. In the restored reach, we evaluated 2 patches with 208-210 grains measured per patch.

Subsurface saturated hydraulic conductivity was estimated at baseflow (August 24th and 29th) using a falling head test following Horslev (1951). 500 mL of water was poured into each piezometer (n=82) and well (n=12) equipped with a pressure transducer (Solinst 3001 Levelogger Junior Edge M10, Georgetown, ON, Canada) recording water levels at a 1-second interval until a baseline water height was reached. The Horslev method estimates the decay of the drawdown ratio of an elevated water height to baseline water height, described by the following equation from Schwartz & Zhang (2003):

$$H_t = H_o * \exp(-KF/A * t) \quad \textbf{(1)}$$

Where A is the cross-sectional area of the well, K is the hydraulic conductivity and F is a shape factor describing the well or piezometer design (here, $F = \frac{11\,R}{2}$ for a cased hole of radius R with soil flush with the bottom), and H_t and H_0 are the drawdown ratios at times t_o *and* t_2 (Schwartz & Zhang, 2003). We estimated K by fitting the observed drawdown ratio at all times with equation (1) using a Marquart-Levenberg technique.

3.4 Quantification of lateral and vertical exchange

To quantify lateral exchange dynamics, each reach was instrumented with three well transects. Transects consisted of two shallow groundwater wells, manually driven into riparian zones with a steel driving rod to approximately 1.5-meters depth. Along the transect we also installed one in-stream stilling well, mounted on a T-post and sited 1-2-meters downstream of the groundwater wells to account for down-valley movement of water along subsurface flowpaths. Wells were constructed from 3.81cm PVC pipe, horizontally screened along the entire subsurface length. The total potential in the wells was measured as the water surface elevation and was characterized hourly, from spring runoff to base flow, using continuously recording water level meters (Solinst 3001 Levelogger Junior Edge M10, Georgetown, ON, Canada). We calculated lateral hydraulic gradients ($\frac{dh}{dl}$)and specific discharge (q) between groundwater and stilling wells to determine the

direction (towards or away from the stream) and flux of groundwater flow:

$$\boldsymbol{q} = -k_{sat}\left(\frac{dh}{dl}\right) \quad \textbf{(2)}$$

Where k_{sat} is saturated hydraulic conductivity dh is the change in total potential measured in the groundwater and stilling wells, dl is the distance between points.

To estimate vertical exchange between the channel and the hyporheic zone, we instrumented the reaches with 41 nested pairs of in-stream piezometers (degraded=18 pairs, restored n=23 pairs). The piezometers were constructed from 2.54 cm PVC, screened along the bottom 1 cm, and manually driven into the bed using a steel driving rod and post pounder. Piezometer nests were sited in the thalweg at 5-10 meter intervals that captured transitions between bed features (e.g. pools, riffles) expected to induce upwelling or downwelling (and later characterized by local slope). Each piezometer nest was comprised of a piezometer driven to 20 cm and 50 cm below the bed surface. We purged the piezometers of fine sediments using a drill pump at low speed, and they were allowed to equilibrate for one week before sampling. Head within the piezometers and relative stream stage were synoptically sampled six times during the study period with a water level meter (Solinst Mini Water Level Meter, Model 102M, Solinst Canada Ltd. Georgetown, ON, USA). Similar to the wells, total head in piezometers was measured as the water surface elevation within the piezometer. We calculated the vertical hydraulic gradient and specific discharge for shallow flowpaths (20 cm to the bed surface, measured as the height of the stream water surface) and deep flowpaths (50 cm to 20 cm below the bed) using **Eq. 2** above, where dl is the vertical distance between points, measured from the base of the paired piezometers.

To evaluate the influence of feature scale (e.g. cobble vs. large riffle) on patterns of vertical, subsurface exchange, we compared pieziometric vertical hydraulic gradients to the local slope of the area upstream of the piezometer nest. A positive bed slope (e.g. riffle) is generally associated with downwelling, while a negative slope (e.g. pool) is associated with upwelling. To account for different scales of topography inducing vertical exchange, we varied the distance across which slope was calculated from small bed undulations (0.5 meters) to large bedforms (5-15 meters). We also wanted to represent the variable length of large bedforms. Because piezometers were intentionally sited to capture changes in bed slope associated with vertical exchange, we used the average slope between piezometers as our variable length scale for analysis. We plotted vertical

hydraulic gradients against this range of local bed slopes and fit regression lines to each relationship. All regressions were tested for significance ($p=<0.05$) and significant results were compared in terms of their resulting r^2 values. The length scale resulting in the best fit (highest r^2), was interpreted as being the feature scale driving vertical exchange.

3.5 Well, Piezometer and Stream Specific Conductance

Environmental tracers can be used to determine the sources, fractions and residence times of water flowing along different subsurface paths. By comparing the chemical composition of stream water source endmembers (e.g. groundwater, soil water) we can evaluate streamflow composition, timescales of transport and degree of exchange (e.g. Sheets et al. 2002; Wett et al. 2002 Hooper et al. 1997; Rice and Hornberger 1998; Cook and Herczeg 2000; Hoeg et al. 2000). Specific conductance (SC) measures water's ability to conduct an electrical charge, and is used as a proxy for the concentration of dissolved ions in solution. As water travels through the subsurface, dissolved ions are accumulated, generally resulting in increased SC with increased contact time (Pilgrim et al. 1979). Here, we use SC as a simple tool to evaluate relative residence time and flushing behaviour in the subsurface. SC measurements were collected using a handheld YSI EC 300 probe (YSI Environmental, YSI Incorporated, Yellow Springs, OH, USA) from wells (n=12), in-stream piezometers (n=82) and stream sources (n=42) during each of the six synoptic surveys. We also identified four groundwater seeps which were measured 2-3 times over the study period. Prior to measurement, wells and piezometers were slowly pumped with a drill-powered, peristaltic pump until 2x the water volume had been flushed.

3.6 Stream Tracer Experiments: Net Change in Discharge and Transient Storage

We used dilution gauging (Day, 1976) to measure discharge (Q) and transient storage at the reach and sub-reach scales. The net change in discharge (dQ) represents the net flux of water (gains plus losses) between the surface and subsurface systems over a given stream or valley length (dx):

$$Net\ change\ in\ discharge\ = \frac{dQ}{dx} \quad \textbf{(3)}$$

A positive net change in flow, therefore, indicates a net gaining stream, where more water is discharging to the stream from the adjacent valley bottom and hyporheic zone than is being lost from the stream. We divided each reach into three consecutive sub-reaches (53-120m length) and collected discharge measurements at each sub-reach boundary, six times over the study period.

Dilution gauging methods apply conservation of mass principles to measure instantaneous discharge at a given location. A known mass of NaCl was injected upstream of a sub-reach boundary. At the downstream measurement location, an electrical conductivity probe, attached to a datalogger, measured the SC breakthrough curve (BTC) as the salt solution passed (Campbell CR1000 data logger and CS-547A temperature/conductivity probe, Campbell Scientific, Inc., Logan, Utah, United States). By integrating under the breakthrough curve, we calculate discharge (**Eq. 4**, from Covino et al., 2011) at each measurement location using a previously quantified linear relationship between SC and Cl^- (1 uS cm^{-1} increase in SC relates to 0.5 g $liter^{-1}$ NaCl):

$$Q = \frac{T_{MA}}{\int_0^t T_c(t)dt} \quad \textbf{(4)}$$

where Q is discharge, T_{MA} is the tracer mass (NaCl) added and T_c is the background corrected tracer concentration. Even mixing of the salt solution throughout the water column is imperative for reliable measurements, so a mixing length (variable length, dependent on discharge) was included upstream of the reach boundary and Rhodamine dye was co-injected to visually assess mixing. To calculate precision error in our discharge measurements, we performed two replicate injections per flow stage, injecting a second NaCl slug after the first injection had passed and baseline SC had been maintained for at least 10 minutes. We then compared the resulting discharge estimates. The repeatability of our dilution gauging measurement was 4.3% of discharge (maximum error 7.6%, minimum error 0.2% of discharge).

Tracer BTC's were also analyzed to quantify advective velocity and transient storage based on the rising and tailing behavior of curves (Harvey et al. 1996). We collected three measurements per reach (along each sub-reach) at 6 flow stages. Advective velocity was calculated as the injection mixing length divided by the elapsed time from injection to peak concentration (t_p). Transient storage was evaluated following methods from Patil et al. (2013), quantifying BTC tailing behavior. We normalized each curve by peak concentration (to account for different masses of NaCl injected) and time to peak (to account for different mixing lengths). The breakthrough curve tail was defined as all concentration measurements from t_{start} to t_{end} where t_{end} was the time where background concentration in reestablished and t_{start} was the midpoint between time of peak concentration (t_p) and t_{end} (Patil et al 2013):

$$t_{start} = t_p + \frac{t_{end} - t_p}{2}$$

(5)

This concentration breakthrough curve tail was then fit with an exponential function*:*

$$C = C_0 e^{-rt}$$

(6)

where (C_0) is the peak concentration, *t* is time and *r* is the exponential decay coefficient that represents tailing behavior. In this case, an *r* value closer to zero (low slope of the breakthrough curve tail) represents more extended tailing behavior, thus higher transient storage. We normalized *r*-values by velocity to allow for comparisons across the different flow periods.

3.7 ^{222}Radon: Groundwater discharge modeling

^{222}Radon (hereafter referred to as radon) is commonly used as a tracer for estimating groundwater discharge to surface water systems. It is a naturally occurring gas produced through the uranium decay series with a 3.82-day half-life. Radon is produced in aquifer sediments and its concentration is regionally variable. As groundwater moves through the aquifer, radon is rapidly accumulated until a maximum concentration is reached and maintained at secular equilibrium (where the rate of production equals the rate of radioactive decay). Because radon is not present in the atmosphere, any contact with the atmosphere initiates degassing from the water body. These properties allow us to distinguish groundwater and stream water end members and approximate groundwater discharge into a stream based on the change in radon concentration over a given stream length.

3.7.1 Radon sampling methods

Synoptic sampling of stream water occurred five times from May-November 2016 at the upstream and downstream extent of degraded and restored reaches. Samples were collected in 250 mL, sample-rinsed glass bottles. Alluvial aquifer samples were collected from floodplain wells and in-stream piezometers three times over the same period using a peristaltic pump. Prior to sample collection, wells and piezometers were pumped at a low rate until 2x the initial volume had been purged.

Radon concentration was measured using a solid state alpha detector (RAD7 with $RADH_20$ accessory unit, Durridge Company Inc, Billerica, MA, USA). To quantify instrument counting

error (the largest potential source of error in estimating radon concentrations), we collected five replicate samples each at high and low flow periods. At average radon concentrations of 127 Bq m^{-3} and 570 Bq m^{-3}, the percent error associated with one standard deviation from the mean was 42% and 5% respectively. We assumed a linear relationship between concentration and error to estimate error at interim radon concentrations.

3.7.2 Radon modeling theory

To estimate groundwater seepage into Ninemile Creek, we applied a one-dimensional advective transport model adapted from Cook et al. (2006). The discharge mass balance over a given length is the sum of inflows (*I*), outflows (O) and evaporative loss (*E*) over stream length x:

$$\frac{dQ}{dx} = I(x) - O(x) - E(x) \quad \textbf{(7)}$$

The measured change in radon concentration over that reach was used to calculate groundwater inflows (*I*, in m^3 day^{-1}meter $stream^{-1}$), accounting for gas exchange with the atmosphere, in-stream radioactive decay and production and decay in the hyporheic zone. The change in radon concentration *(c)* over distance *(x)* is given by (Cook et al. 2006):

$$Q\frac{dc}{dx} = I(c_i - \underline{c}) + wE\underline{c} - kw\underline{c} - dw\lambda\underline{c} + \frac{\gamma hw\theta}{1+\lambda t_h} - \frac{\lambda hw\theta}{1+\lambda t_h}\underline{c} \quad \textbf{(8)}$$

where c_i is the radon concentration in groundwater [Bq m^{-3}] , $\underline{c}$ is the mean concentration between upstream and downstream measurement points [Bq m^{-3}], *w* is channel width [m], *d* is the channel depth [m], *k* is the gas transfer velocity [m day-^{1}], λ is the decay coefficient [day^{-1}], *y* is production of radon in the hyporheic zone [Bq m^{-3} day^{-1}], *h* is the depth of the hyporheic zone [m] and θ is the porosity of the hyporheic zone.

We assumed spatial homogeneity for each of our parameters, and steady-state flow conditions at each measurement time interval. By using $\underline{c}$ to represent in-stream radon concentrations, we adopt a mixing model approach, assuming that the change in radon over the reach length is linear. We assume that the hyporheic zone is homogenous, well mixed and that the mean HZ residence time is representative of the existing range of flow path residence times (Cook et al., 2006;

Bourke et al., 2014). Within the stream, we assume even mixing of radon in the water column and that diffusion of radon from sediments is negligible with respect to the influence of advective fluxes of radon from groundwater or hyporheic sources.

It is important to note that the "groundwater" signature of radon at secular equilibrium is present in any water with a subsurface residence time greater than approximately two weeks. This means that regional groundwater is indistinguishable from most bank storage or parafluvial sources. "Groundwater," in this model, is therefore defined as alluvial aquifer water that has reached secular equilibrium. This is in contrast to short, hyporheic flow paths. Hyporheic exchange can affect in-stream radon concentrations, as seen in the final two terms of **Eq. (8)**.

3.7.3 Parameterization and radon modeling methods

To evaluate temporal trends in groundwater discharge on restored and degraded reaches of Ninemile Creek, we approximated **Eq. (8)**, discretizing our model over the full reach length and applying the selected parameter values (Appendix A, Table 1). We then optimized our model to match observed upstream and downstream radon concentrations by manipulating *I*. Groundwater discharge flux was modeled for each reach, at each of the five time intervals from May-November 2016.

Direct measurements of stream radon concentrations, stream discharge and stream channel dimensions provided reliable estimates of these parameters and their associated errors. Gas exchange and hyporheic zone (HZ) parameters were more challenging to accurately estimate. Because they were not directly measured, a reasonable range of values was determined for each, informed by existing literature and field measurements of associated parameters. A series of sensitivity analyses were conducted to evaluate model response to any parameter that was not measured directly. Each unknown parameter was allowed to vary over its estimated range, holding all other parameters constant. We modeled each equation independently, manually adjusting *I* to match measured *dc/dx* values. The range in *I* resulting from this variation provides insight into the sensitivity of the model to that parameter.

Accurate estimates for gas exchange velocity is especially difficult in low-order streams with highly variable geometry, velocity and temperature. Because *k* was not measured in the field, we placed a special emphasis in evaluating the sensitivity of our model to *k*. We used four common equations (Appendix A, Table 2) to approximate *k* and applied the mean of the results for each

sampling period to our final model. All equations rely on physical measurements of velocity (*V),* slope (*S*) and depth *(D)* which were measured at the project site throughout the season.4.

RESULTS

4.1 Seasonal streamflow and precipitation response:

Precipitation and discharge trends followed a pattern typical of snowmelt-dominated mountainous regions, with peak flows associated with basin snowmelt in April and May, and rain events (June, July and October) that contributed to coincident rises in stream discharge (Appendix A, Figure 3). Baseflow occurred in September and was preceded by a period of 6-weeks with minimal precipitation. Average stream discharge measured on our sampling dates (dashed lines in Appendix A, Figure 3) were 666, 411, 292, 156, 112 and 149 l sec^{-1} for May 24th, June 9th, July 7th, August 17th, September 14th and November 4th respectively.

Regional snow water equivalent reached 34 cm, 86% of the median for the period of record (measured at the Sleeping Woman SNOTEL site). The date of peak snow water equivalent was consistent with the historic record (first week of April), but the last day of recorded snowpack was May 4th, 23 days before the median historic date of full melt. Precipitation accumulation was at, or slightly above, the historic median throughout the study period.

4.2 Physical characterization of restored and degraded sites

Analysis of topographic and geomorphic survey data revealed notable differences between the restored and degraded reaches (Appendix A, Figure 4 and 5, Table 3). The restored reach exhibited increased sinuosity, bed complexity width-to-depth ratios. Sinuosity increased from 1.05 in the degraded reach to 1.33 in the restored reach. This added stream length resulted in a 50% decrease in stream slope, from 0.015 to 0.010. Width-to-depth ratios increased from 12 in the degraded reach to 18 in the restored reach. Bed complexity was higher in the restored reach, with a lower r^2 value (0.927 vs. 0.978) and higher standard deviation of residuals (32.4 vs. 10.3) when a regression line was fit to the surveyed longitudinal profiles.

Textural analysis of the stream bed (Appendix A, Figure 5a) revealed that the restored reach had a coarser composition overall, most notably in the large cobble-small boulder size classes (>128mm) which comprised 49% of grains sampled in the restored reach and only 30% in the degraded reach. The restored reach median grain size was 90 mm (cobble) in contrast with 64 mm (large pebble) in the degraded reach. Finer grain size classes were similar between reaches.

Grains 2.0-5.6 mm (sand-granule) made up of 7% of the total grains sampled in both reaches. The degraded reach had 4% more silt and sand (< 2 mm), but most of these samples occurred in the pool upstream of the beaver dam. Discounting the beaver dam, silt and sand comprised only 1% of the total grain size distribution of the bed surface in both reaches.

Analysis of the saturated hydraulic conductivity of subsurface stream sediments from piezometers (Appendix A, Figure 5b) shows that the restored reach had a lower median conductivity and lower variability at both 20 and 50 cm depths. Median hydraulic conductivities in the restored reach were 8.6 cm hr^{-1} (50 cm depth) and 52.2 cm hr^{-1} (20 cm depth), in contrast to 14.5 (50cm depth) and 367.6 cm hr^{-1} (20 cm depth) in the degraded reach. The interquartile range of conductivities at 20 cm and 50 cm depth were 58.7 and 137.6 cm hr^{-1} in the restored reach and 308.2 and 462.8 cm hr^{-1} in the degraded reach. There was also a clear differentiation between hydraulic conductivities at 20 and 50 cm for both treatments, with higher conductivity at shallower depths. This stratification was particularly evident in the degraded reach (difference between median values = 353.1 cm hr^{-1} in degraded and 43.6 cm hr^{-1} in restored).

4.3 Exchange

4.3.1 Advective velocity and transient storage

Analyses of dilution gauging breakthrough curves showed 5-34% lower in-stream mean velocities for the restored reach at moderate to low flows. At the highest measured flows (May), the velocity in the restored reach was 11% higher than in the degraded reach (Restored monthly mean velocity: 0.89, 0.68, 0.45, 0.26, 0.29, 0.39 m sec^{-1}; Degraded monthly mean velocity: 0.80, 0.72, 0.57, 0.39, 0.39, 0.48 m sec^{-1}). When we consider velocity in terms of the valley length, describing the rate of surface water movement out of the valley bottom, values were 8-48% lower in the restored reach due to increased sinuosity (Restored monthly mean velocity: 0.66, 0.50, 0.33, 0.19, 0.20, 0.28 m valley sec^{-1}; Degraded 0.71, 0.68, 0.53, 0.37, 0.37, 0.46 m valley sec^{-1}).

We evaluated transient storage at peak (May), moderate (June) and low (September) flows (Appendix A, Figure 6). Transient storage in the restored sub-reaches was higher (*r*-values closer to zero) than degraded sub-reaches (Appendix A, Figure 6). Transient storage in the degraded reach increased as streamflow decreased (mean of *r*-values = -0.031, -0.028 and -0.026 for May, June and September respectively). In the restored reach, transient storage was consistent at high and moderate flows (-0.014 and -0.015 for May and June), decreasing at base flow (-0.017 in

September). Transient storage in the degraded reach was consistently highest in the beaver dam sub-reach (circled in black in Appendix A, Figure 6). When these values were removed from consideration, transient storage in the degraded reach was further decreased (mean of r-values = -0.034, -0.033, -0.030 for May, June and September).

4.3.2 Vertical exchange

Vertical hydraulic gradients were similar between the restored and degraded reaches (Appendix A, Figure 7). In both reaches, there was a clear separation of gradients by flowpath depth, with deeper flowpaths dominantly downwelling (median gradient by month degraded: -0.19, -0.14, -0.09, -0.11, -0.01, -0.11; median gradient by month restored: -0.11, -0.11, -0.15, -0.17, -0.02, -0.12) , and shallow flowpaths generally exhibiting an even distribution of upwelling and downwelling (median gradient by month degraded: 0.08, 0.38, 0.08, 0.04, 0.12, 0.03; median gradient by month restored: 0.05, 0.08,0.05, 0.00, 0.04, 0.04).

The length scale of feature inducing vertical exchange differed between reaches. Regardless of the length-scale used to calculate the slope (0-15 meters), the degraded reach showed no significant relationship between vertical hydraulic gradient and local bed slope. In the restored reach, and at shallow depths (0-20 cm), there were significant negative relationships ($p>0.05$) in four of six months and at several length scales (Appendix A, Table 4). We also evaluated slope at a variable length scale to account for the variable lengths of stream bed features. This was defined as the average slope between two subsequent piezometers that were cited to capture changes in slope generally associated with upwelling or downwelling. The variable length scale predicted vertical hydraulic gradients best (highest r^2 value of all significant relationships) in May, July and September (r^2 of 0.20, 0.26 and 0.19 respectively). In November, a 5-meter length provided the best fit ($r^2 = 0.27$). The variable length scale for the restored reach ranged between 7-35 meters, with a mean length of 19 meters. There were no significant relationships in the restored reach in June or August using any length scale of bed slope. Deep flow paths (20-50 cm), which were predominantly downwelling, showed no significant relationships at any time or length scale with the exception of September base flow at the variable length-scale in the restored reach.

Despite the two reaches having similar vertical hydraulic gradients, when we evaluated specific discharge, the degraded reach had a much higher exchange flux due to its higher hydraulic conductivity (Appendix A, Figure 8 a-b). The median absolute value of fluxes in the degraded reach ranged from 80.7 cm hr^{-1} at peak flows to 74.2 cm hr^{-1} at base flow. In the restored reach

the flux values were substantially reduced, ranging from 5.0 cm hr^{-1} to 2.7 cm hr^{-1} at peak and base flows.

4.3.3 Specific Conductance

Mean specific conductance in groundwater seeps was 247 uS cm^{-1} (minimum:167 uS cm^{-1} maximum: 322 uS cm^{-1}) while streamwater ranged from a minium of 154 in May to a maximum of 180 in June. Baseflow SC was 172 in September. SC from subsurface water samples in the restored reach were consistently higher and more variable (20 cm depth: median=191 uS cm^{-1}, range=995 uS cm^{-1}; 50 cm depth: median = 181 uS cm^{-1} range =924 uS cm^{-1}) than the degraded reach (20 cm depth: median=177 uS cm^{-1}, range=149 uS cm^{-1} ; 50 cm depth: median = 185 uS cm^{-1} range =279 uS cm^{-1}) (Appendix A, Figure 8 c-d). In both reaches, median SC values increased with subsurface depth.

4.3.4 Lateral exchange

We analysed lateral gradients of exchange between shallow groundwater wells and the stream to evaluate the direction of flow toward (positive gradient) or away from (negative gradient) the stream. Appendix A, Figure 9 presents hourly gradients at each of the twelve wells over time. The restored reach exhibited neutral to losing (negative) gradients, becoming more negative with the decline in stream stage. The degraded reach, in contrast, consistently gained (positive gradients) in the lateral direction.

4.4 Temporal trends in Groundwater Recharge-Discharge

4.4.1. Base flow discharge modeling using ^{222}Radon

In-stream radon concentrations ranged from a minimum of 146 Bq m^{-3} in May to a maximum of 663 Bq m^{-3} in November. We selected a groundwater radon concentration of 26,250 Bq m^{-3} for our model, which was the maximum radon concentration measured at the site.

Based on our sensitivity analyses, instrument counting error of radon concentration (*c*) produced the broadest range of model outcomes, followed by gas exchange velocity (*k*). Our final model of groundwater inflows (Appendix A, Figure 10a) presents modeled inflows plus or minus one standard deviation of radon concentration measurement error. Results are normalized by valley length to represent the valley-scale impact of restoration. The *k* value used in this model is the mean of the four gas exchange velocity equations. The restored reach demonstrated continuous groundwater inflows to the stream throughout the season (mean inflows: 1.70, 1.65, 0.78, 1.80 m^3

day^{-1} m valley^{-1} for June, July, August and November samples), with 88-100% higher inflows than the degraded reach in July-November. The clear exception to this is in June, when the degraded reach shows a 17% higher inflow rate, which rapidly declines towards zero inflows by August (mean degraded inflows: 2.05, 0.20, 0.00, 0.10 m^3 day^{-1} m valley^{-1} for June, July, August and November samples). In August, at lowest sampled streamflow, the restored reach had an inflow flux of 0.78 m^3 day^{-1} m valley^{-1} while the degraded reach had 0.00 m^3 day^{-1} m valley^{-1}.

4.4.2 Net change in discharge

We also used net change in discharge from upstream to downstream to evaluate recharge and discharge dynamics over time (Appendix A, Figure 10b). Similar to the radon model, the degraded reach was gaining in June, with gains declining throughout the season until September base flow, when the net change in discharge was close to neutral (13.7, 15.3, 8.5, -0.4, 6.5 m^3 day^{-1} m valley^{-1} in June-November). The restored reach, in contrast, gained in early spring, then lost water during the early summer. As base flow approached in August, this dynamic switched, with the restored reach gaining groundwater as flows receded (0.65, -5.6, 6.5, 4.6, 2.0 m^3 day^{-1} m valley^{-1} in June-November). At September base flow, the degraded reach was losing (-0.4 m^3 day^{-1} m valley^{-1}), while the restored reach maintained gains of 4.6 m^3 day^{-1} m valley^{-1}.

5. DISCUSSION

Restoration altered hydraulic exchange processes across all spatial scales evaluated. Our results suggest 1) Increased in-stream residence time and transient storage 2) Initiation of feature-scale vertical exchange (though limited by substrate stratification) 3) Reduced vertical flux due to lower hydraulic conductivity and 4) Temporal shifts in lateral exchange dynamics, with more neutral to losing (storing) trends in the restored reach. Cumulatively, these changes in hydraulic exchange processes altered temporal patterns of alluvial aquifer recharge and discharge. These results were consistent with our conceptual model, showing increased early-season storage which later subsidized base flow. In the following sections, we discuss how physical alterations to the restored reach morphology led to differences in hydrologic exchange and reach-scale storage and discharge dynamics.

5.1 Effects of Restoration on Hydraulic Exchange

5.1.1 Advective velocity and transient storage

Restoration decreased velocity and increased transient storage at nearly all flow stages. This is clearly illustrated in our transient storage results, showing longer tailing behavior associated with back-eddies and short-term hyporheic flowpaths (Appendix A, Figure 6). While we do not have distributed data to link these trends to structural changes, we know that restoration increased the complexity of the channel in multiple dimensions (including sinuosity and bedform), while decreasing slope (Appendix A, Figure 4, Appendix A, Table 3). Each of these channel characteristics has been linked to increased transient storage, slowing and recirculating surface water within the channel and reducing the influence of advection (Gooseff et al., 2007; Harvey et al., 2003; Patil et al.,2013; Salehin et al., 2003; Wondzell, 2006). This type of exchange is crucial for short-term processes like biogeochemical transformations (Boulton et al. 1998; Findlay, 1995) but likely has little effect on seasonal trends in storage and baseflow discharge.

5.1.2 Vertical exchange

Our results highlight the importance of considering substrate hydraulic conductivity in conjunction with streambed topography when attempting to modify hyporheic exchange flows. The addition of larger streambed features (e.g.riffles, pools) did lead to predictable spatial patterns of upwelling and downwelling (Appendix A, Table 4) that were not observed in the degraded reach. However, this exchange was limited to the upper 20 cm of the subsurface. There was no evidence to suggest that the constructed features promoted the deeper flowpaths with longer residence times that have been observed in other field and model simulations (Marzadri et al., 2014; Stonedahl et al. 2010; Tonina & Buffington, 2011). We attribute this to the overall lower, and stratified hydraulic conductivity of the subsurface. Lower hydraulic conductivity was likely a result of compaction from the construction process that reduced median vertical flux in the shallow zone by 93-96%. In the degraded reach, we found no relationship between local bedslope and longitudinal patterns of upwelling and downwelling. This suggests that here, vertical exchange is controlled by features smaller than 50 cm (the resolution limit of our analysis), or by other factors such as heterogeneity in the substrate hydraulic conductivity. Stratification of the subsurface was particularly evident in the degraded reach (Appendix A, Figure 5b), resulting in higher fluxes in the upper 20 cm zone. These results are also supported by our SC data. SC in the degraded reach at 20 cm was similar to streamwater with little variance, indicating rapid flushing and little interaction with the substrate (Appendix A, Figure 8 c-d). In

the restored reach, at both 20 and 50 cm depths, SC was higher, more variable, and increased with depth. This suggests that longer subsurface residence times allowed for increased weathering reactions and/or mixing with solute-rich groundwater sources.

5.1.3 Lateral Exchange

The patterns of lateral groundwater-surface water exchange measured by our monitoring wells were consistent with our conceptual model. The degraded reach showed lateral gradient trends typical of an incised channel (Schilling et al. 2004) (Appendix A, Figure 9a). Throughout the year, the alluvial aquifer discharged to the degraded stream due to the gradient produced by an unnaturally low channel elevation. This lowered elevation eliminated bank storage processes at high flows and contributed to more rapid drainage of the alluvial aquifer (similar to results of Schilling et al. 2006). The restored reach, in contrast, had neutral to losing gradients throughout the season (Appendix A, Figure 9b). Losses from the stream generally indicate alluvial aquifer recharge, while relatively neutral gradients may be indicative of dominant subsurface flow running parallel to the channel (underflow, sensu Larkin and Sharp, 1997), rather than in the lateral direction. Our instrumentation design did not directly evaluate the impact of increased sinuosity on parafluvial flow or underflow, but we believe that this was likely a substantial exchange process affected by restoration. This is supported by the generally neutral lateral gradient observed, as well as a wealth of literature showing a positive relationship between the degree of channel curvature and exchange flux through bars and banks (e.g. Boano et al. 2006; Cardenas et al., 2009; Gomez et al., 2012; Stonedahl et al., 2010).

5.2 Temporal trends in alluvial aquifer recharge and discharge

Temporal trends in alluvial aquifer recharge and discharge were markedly different in the restored and degraded settings. Overall, our results support the hypothesis that restoration induced alluvial aquifer storage during spring snowmelt, allowing for more sustained and higher volumetric discharge at low flows. By comparing seasonal trends in lateral gradients to radon modeling and net change in discharge results, we can begin to elucidate the mechanisms behind the recharge-discharge dynamics observed.

In June, the Ninemile basin was likely contributing a maximum amount of water to the Ninemile valley due to Spring snowmelt and precipitation. Our radon modeling, net change in discharge and lateral gradient results all indicate that in the degraded reach, this water moved rapidly into the stream system, causing high rates of groundwater discharge to the stream which rapidly

declined as the season progressed (Appendix A, Figures 9 and 10). These results align with results from Huntington and Niswonger (2012) showing maximum groundwater discharge following peak stream stage. In the restored reach, however, our radon model shows a buffered response to hillslope contributions, with lower early-season inflows compared to the degraded reach (Appendix A, Figure 10a). This suggests that contributions from hillslopes and bank storage were stored, producing the more gradual decline in alluvial aquifer discharge through the base flow recession. Net change in discharge results also support this observation, showing losses (storage) early in the season, shifting to gains (discharge) that sutained base flows (Appendix A, Figure 10b). Of particular importance, both metrics show substantially higher volumetric discharge at the lowest measured streamflows (increase of 0.7 m^3 day^{-1} m $valley^{-1}$ of radon-modeled groundwater discharge, and 5 m^3 day^{-1} m $valley^{-1}$ net gains).

These trends generally agree with lateral gradient results, supporting our hypotheses that by reducing the elevation differential between the channel and floodplain, restoration neutralizes lateral gradients and increases the duration of the seasonal storage period. Dominant trends of storage and underflow in the restored reach fit our conceptual model (Appendix A, Figure 1) except at base flow where we would expect to see a reversal in the lateral gradient direction, with stored water discharging into the stream (as indicated by radon and net change in flow results). This inconsistency is most likely explained by well placement. Lateral gradient data was derived from six point measurements that may not be representative of the lateral dynamics of the reach as a whole. Two of the six locations have gradients towards the stream in September and may, therefore, represent key outflows of stored water that are supporting base flow.

5.3 Restoration Implications: Transferring results outside of the Ninemile Creek Basin

Stream restoration projects are generally designed to meet several, concurrent ecological goals including habitat enhancement, thermal regulation or water quality improvement through erosion control or increased biogeochemical processing. Each of these processes is intrinsically linked to hydraulic exchange. However, the flowpath length of maximum benefit varies depending on the process being considered. For example, frequent, shallow exchange delivers a consistent flow of dissolved oxygen to the near-bed hyporheic zone, essential to ecological processes such as nutrient assimilation or incubation of fish eggs. These short flow paths, however, have limited influence on stream temperatures or valley-scale retention when compared to longer-duration flowpaths (Arrigoni et al. 2008, Brunke and Gosner, 1997; Helton et al. 2014; Cardenas, 2007;

Poole et al., 2006).

Our work focused on base flow generation, which is linked to the creation of larger-scale features inducing longer-duration flowpaths. This includes reducing channel incision (resulting in a lower lateral gradient between the stream and valley, increasing bank storage and slowing drainage), increasing sinuosity (widening the extent of the interactive alluvial aquifer and promoting underflow through longer, down-valley flowpaths) and inclusion of larger-scale vertical features like woody debris dams or beaver dams (inducing deeper vertical flux). It is unlikely that smaller geomorphic features will have a significant impact on baseflow, but their value in providing other ecological services is paramount. In this sense, increasing the *variability* of hydraulic exchange paths should be considered as an overarching restoration goal (Kondolf et al. 2006).

If we accept the goal of achieving variable flowpath lengths, it's important to consider how not only topography, but also hydraulic conductivity, affects flowpath length and residence time. Our vertical exchange results provide a key example. Compaction in the restored reach likely caused the low hydraulic conductivity reduced vertical flux observed. This impact could be minimized or avoided during construction. However, substrate stratification (also seen in the degraded reach) may be a natural result of fluvial sorting of the bed material material. In another system with more conductive, homogeneous alluvial material, construction of variable topography will induce deeper flowpaths. In systems like the Ninemile, the impact of these features is limited. Instead, flowpath length and residence time was strongly influenced by the hydraulic conductivity and the potential for substrate stratification. Heterogeneity in both topography and hydraulic conductivity will likely result in power law residence times distributions with concurrent short, medium and long flowpaths, even though the mechanisms driving these distributions differ. More work is needed to understand how ecological processes like nutrient uptake length, or physical processes like heat transfer, are impacted depending on the mechanism driving the exchange flux.

Finally, and perhaps most importantly, it is essential to recognize that the hydrologic response of a stream to restoration will be strongly influenced by factors that valley-bottom restoration cannot impact. Climate, upland topography, lithology and basin form all control the rate, volume, location and timing of inflows into, and out of, the alluvial aquifer (Bergstrom et al., 2016; Harvey and Gooseff, 2015; Jencso et al., 2009; Jencso et al., 2010; Ward et al., 2016). Our research shows that manipulations of the physical form of the alluvial valley and stream can impact exchange and storage dynamics; the restored reach demonstrated predicted changes in

patterns of alluvial aquifer recharge and discharge, resulting in higher volumetric base flow. However, the effect of these manipulations will vary by local conditions. For example, raising the channel bed elevation in a system with minimal inflows from upland sources may result in reduced, or even loss of stream flow if the alluvial aquifer cannot be filled to match the new elevation. This response would clearly have concerning impacts on stream temperatures, habitat and survival of biota. Additionally, the relative effect of restoration on alluvial aquifer storage will decrease as aquifer volume increases. Surficial manipulations of topography, or increases in the volumetric storage capacity of an aquifer can have substantial effects in relatively small, shallow aquifers. In larger, lower-gradient river systems, a comparable effort would result in a much smaller relative increase in exchange and storage.

6. CONCLUSION

In this paper, we quantify the effect of channel restoration on nested scales of hydraulic exchange and temporal patterns of alluvial aquifer recharge and discharge. Using a combination of geomorphic and topographic surveys, hydrometrics, groundwater tracers and discharge measurements, we link changes in the physical form of the channel and valley to hydrologic responses to restoration across spatial and temporal scales. Restoration increased transient storage, likely due to increased sinuosity, bedform complexity and reduced slope. Introduction of larger, more variable bed features (riffles and pools) effectively induced vertical exchange, though the depth and rate of exchange was limited by the lower, stratified hydraulic conductivity. Lateral exchange trends in the restored reach were dominated by storage or underflow processes, in contrast to rapid aquifer drainage (discharge) in the degraded reach.

The cumulative impact of these exchange processes resulted in a longer period of alluvial aquifer recharge early in the season, allowing for higher volumetric discharge to sustain base flow. This is evidenced by net losses in stream discharge (storage) in the restored reach at moderate flows and higher net volumetric gains (discharge) at base flow. Additionally, ^{222}Radon modeling results reveal a more gradual, prolonged reduction in groundwater discharge from Spring to base flow, with higher rates of discharge at most time periods, most notably at the lowest flows.

Our findings support an assumed, but not well examined theory that stream restoration can prolong the baseflow recession, contributing larger volumes of stored alluvial aquifer water to the stream later in the season. This may have significant impacts on streamflow discharge and temperature, especially at base flow. This approach to restoration could, therefore, be effective in

buffering streams from climate change-induced variations in the water cycle. Basin characteristics such as climate, lithology and existing storage capacity must be considered to appropriately characterize how form may influence hydrologic function of disturbed and restored watersheds.

References

Arrigoni, A. S., G. C. Poole, L. A. K. Mertes, S. J. O'Daniel, W. W. Woessner, and S. A. Thomas (2008), Buffered, lagged, or cooled? Disentangling hyporheic influences on temperature cycles in stream channels, Water Resour. Res., 44, W09418, doi:10.1029/2007WR006480.

Barnett, T.P., J.C. Adam and D.P. Lettenmaier (2005), Potential impacts of a warming climate on water availability in snow-dominated regions, Nature, 438, 303-309, doi:10.1038/nature04141

Bencala, K. E., M. N. Gooseff, and B. A. Kimball (2011), Rethinking hyporheic flow and transient storage to advance understanding of stream-catchment connections, Water Resour. Res., 47, W00H03, doi:10.1029/2010WR010066.

Bergstrom, A., Jencso, K., & McGlynn, B. (2016). Spatiotemporal processes that contribute to hydrologic exchange between hillslopes, valley bottoms, and streams. Water Resources Research, 52(6), 4628-4645

Berkowitz, B., Cortis, A., Dentz, M., & Scher, H. (2006). Modeling non- Fickian transport in geological formations as a continuous time random walk. Reviews of Geophysics, 44(2).

Boano, F., Camporeale, C., Revelli, R., & Ridolfi, L. (2006). Sinuosity- driven hyporheic exchange in meandering rivers. Geophysical Research Letters, 33(18).

Boulton, A. J., Findlay, S., Marmonier, P., Stanley, E. H., & Valett, H. M. (1998). The functional significance of the hyporheic zone in streams and rivers. Annual Review of Ecology and Systematics, 29(1),59-81.

Bourke, S.A.', P.G. Cook, M. Shanafield, S. Dogramaci, J.F. Clark (2014) Characterisation of hyporheic exchange in a losing stream using radon-222, Journal of Hydrology, 514(A), 94-105

Brunke, M., & Gonser, T. O. M. (1997). The ecological significance of exchange processes between rivers and groundwater. Freshwater biology, 37(1), 1-33.

Buffington, J. M. and Tonina, D. (2009), Hyporheic Exchange in Mountain Rivers II: Effects of Channel Morphology on Mechanics, Scales, and Rates of Exchange. Geography Compass, 3: 1038–1062. doi: 10.1111/j.1749-8198.2009.00225

Cardenas, M. B. (2007). Potential contribution of topography- driven regional groundwater flow to fractal stream chemistry: Residence time distribution analysis of Tóth flow. Geophysical Research Letters, 34(5).

Cardenas, M. B. (2008). Surface water- groundwater interface geomorphology leads to scaling of residence times. Geophysical Research Letters, 35(8).

Cardenas, M. Bayani. (2009) Stream- aquifer interactions and hyporheic exchange in gaining and losing sinuous streams. Water Resources Research 45.6

Cook, P. G., Lamontagne, S., Berhane, D., & Clark, J. F. (2006). Quantifying groundwater discharge to Cockburn River, southeastern Australia, using dissolved gas tracers 222Rn and SF6. Water Resources Research, 42(10).

Cook, P.G., & A.L. Herczeg (2000), Environmental Tracers in Subsurface Hydrology. Springer US: 2000. Print. 10.1007/978-1-4615-4557-6

Covino, T., McGlynn, B., & Mallard, J. (2011). Stream- groundwater exchange and hydrologic turnover at the network scale. Water Resources Research, 47(12).

Day, T. J. (1976). On the precision of salt dilution gauging. *Journal of Hydrology*, *31*(3-4), 293-306.

E.P.A. 2015. "Connectivity of Streams & Wetlands to Downstream Waters: A Review & Synthesis of the Scientific Evidence." Washington

Findlay, S. (1995). Importance of surface- subsurface exchange in stream ecosystems: The hyporheic zone. Limnology and oceanography, 40(1), 159-164.

Google Inc. (2017). Google Earth (Version 7.1.8.3036). Available from https://www.google.com/earth/

Gomez, J. D., Wilson, J. L., & Cardenas, M. B. (2012). Residence time distributions in sinuosity- driven hyporheic zones and their biogeochemical effects. Water Resources Research, 48(9).

Gooseff, M. N., Anderson, J. K., Wondzell, S. M., LaNier, J., & Haggerty, R. (2006). A modelling study of hyporheic exchange pattern and the sequence, size, and spacing of stream bedforms in mountain stream networks, Oregon, USA. Hydrological Processes, 20(11), 2443-2457.

Gooseff, Michael N., Robert O. Hall, and Jennifer L. Tank. (2007) Relating transient storage to channel complexity in streams of varying land use in Jackson Hole, Wyoming." Water Resources Research 43.1.

Green, T.R., M. Taniguchi, H. Kooi, J.J. Gurdak, D.M. Allen, K.M. Hiscock, H. Treidel, A. Aureli (2011) Beneath the surface of global change: Impacts of climate change on groundwater, Journal of Hydrology, 405, 532-560

Hammersmark, C.T., M.C. Rains, and J.F. Mount. (2008) Quantifying the hydrological effects of

stream restoration in a montane meadow, northern California, USA." River Research and applications 24.6: 735-753.

Harvey J.W. and K.E. Bencala (1993), The effect of streambed topography on surface-subsurface water exchange in mountain catchments, Water Resour. Res., 29(1), doi: 10.1029/92WR01960.

Harvey, J. W., Conklin, M. H., & Koelsch, R. S. (2003). Predicting changes in hydrologic retention in an evolving semi-arid alluvial stream. Advances in Water Resources, 26(9), 939-950.

Harvey, J., and M. Gooseff (2015), River corridor science: Hydrologic exchange and ecological consequences from bedforms to basins, Water Resour. Res., 51, 6893–6922,

Harvey, J. W., B. J. Wagner, and K. E. Bencala (1996), Evaluating the reliability of the stream tracer approach to characterize stream-subsurface water exchange, *Water Resour. Res.*, 32(8), 2441–2451

Hauer, F. Richard, et al. (2016) Gravel-bed river floodplains are the ecological nexus of glaciated mountain landscapes. Science Advances 2.6

Helton, A. M., Poole, G. C., Payn, R. A., Izurieta, C., & Stanford, J. A. (2014). Relative influences of the river channel, floodplain surface, and alluvial aquifer on simulated hydrologic residence time in a montane river floodplain. Geomorphology, 205,
17-26.

Hester, E. T. and Gooseff, M. N. (2011) Hyporheic Restoration in Streams and Rivers, in Stream Restoration in Dynamic Fluvial Systems (eds A. Simon, S. J. Bennett and J. M. Castro), American Geophysical Union, Washington, D. C.

Hoeg, S., Uhlenbrook, S., & Leibundgut, C. (2000). Hydrograph separation in a mountainous catchment—combining hydrochemical and isotopic tracers. Hydrological Processes, 14(7), 1199-1216

Hooper, R., B. Aulenbach, D. Burns, J. J. McDonnell, J. Freer, C. Kendall, and K. Beven (1997), Riparian control of streamwater chemistry: Implications for hydrochemical basin models, IAHS Redbook, 248, 451–458.

Hvorslev, M. J. (1951). Time lag and soil permeability in ground-water observations.

Hill, A. R. (1996), Nitrate removal in stream riparian zones, J. Environ. Qual., 25, 743–755.

Huntington, J. L., & Niswonger, R. G. (2012). Role of surface- water and groundwater interactions on projected summertime streamflow in snow dominated regions: An integrated modeling approach. Water Resources Research, 48(11).

IPCC, 2014: Climate Change 2014: Synthesis Report. Contribution of Working Groups I, II and III to the Fifth Assessment Report of the Intergovernmental Panel on Climate Change [Core Writing Team, R.K. Pachauri and L.A. Meyer (eds.)]. IPCC, Geneva, Switzerland,

Jencso, K., B. McGlynn, M. Gooseff, S. Wondzell, K. Bencala, and L. Marshall (2009), Hydrologic connectivity between landscapes and streams: Transferring reach-and plot-scale understanding to the catchment scale, Water Resour. Res., 45, W04428,

Jencso K.G., B.L. McGlynn, M.N. Gooseff, K.E. Bencala and S.M. Wondzell (2010), Hillslope hydrologic connectivity controls riparian groundwater turnover: Implications of catchment structure for riparian buffering and stream water sources, Water Resour. Res., 46,

Kasahara, T., Mutz, M., and Boulton, A. J. (2009) Treating causes not symptoms: restoration of surface–groundwater interactions in rivers. Marine and Freshwater Research 60, 976–981.

Kondolf, G. M., A. J. Boulton, S. O'Daniel, G. C. Poole, F. J. Rahel, E. H. Stanley, E. Wohl, A. Bång, J. Carlstrom, C. Cristoni, H. Huber, S. Koljonen, P. Louhi, and K. Nakamura (2006) Process-based ecological river restoration: visualizing three-dimensional connectivity and dynamic vectors to recover lost linkages. Ecology and Society11(2): 5.

Kim, J. S., & Jain, S. (2010). High-resolution streamflow trend analysis applicable to annual decision calendars: A western United States case study. Climatic change, 102(3), 699-707.

Larkin and Sharp (1992) On the relationship between river-basin geomorphology, aquifer hydraulics, and ground-water flow direction in alluvial aquifers. GSA Bulletin Dec 1992, 104 (12) 1608-1620

Luce, C. H., & Holden, Z. A. (2009). Declining annual streamflow distributions in the Pacific Northwest United States, 1948–2006. Geophysical Research Letters, 36(16).

Marzadri, A., Tonina, D., McKean, J. A., Tiedemann, M. G., & Benjankar, R. M. (2014). Multi-scale streambed topographic and discharge effects on hyporheic exchange at the stream network scale in confined streams. Journal of Hydrology, 519, 1997-2011.

Montana Bureau of Mines and Geology, Montana Tech, University of Montana Availaible online at http://mbmg.mtech.edu/mbmgcat/public/ListArchives.asp. Accesses [01/14/2016]

Montgomery, D.R. and J.M. Buffington (1997), Channel-reach morphology in mountain drainage basins, GSA Bulletin, 109(5), 596-611.

Moore, J. N., Harper, J. T., & Greenwood, M. C. (2007). Significance of trends toward earlier snowmelt runoff, Columbia and Missouri Basin headwaters, western United States. Geophysical Research Letters, 34(16).

Natural Resources Conservation Service, United States Department of Agriculture. Web Soil Survey. Available online at https://websoilsurvey.sc.egov.usda.gov/. Accessed [11/06/2015].

Negulescu, M., and V. Rojanski. (1969) Recent research to determine reaeration coefficient. Water Research 3.3: 189IN3193-192IN6202.

O'Connor, D. and W. Dobbins. 1958. Mechanism of reaeration in natural streams. Transactions of the American Society of Civil Engineers 123:641–684.

Patil, S., Covino, T. P., Packman, A. I., McGlynn, B. L., Drummond, J. D., Payn, R. A., & Schumer, R. (2013). Intrastream variability in solute transport: Hydrologic and geomorphic controls on solute retention. Journal of Geophysical Research: Earth Surface, 118(2), 413-422.

Payn, R. A., Gooseff, M. N., McGlynn, B. L., Bencala, K. E., & Wondzell, S. M. (2012). Exploring changes in the spatial distribution of stream baseflow generation during a seasonal recession. *Water Resources Research*, *48*(4).

Pilgrim, D. H., Huff, D. D., & Steele, T. D. (1979). Use of specific conductance and contact time relations for separating flow components in storm runoff. *Water Resources Research*, *15*(2), 329-339.

Poole, G. C., Stanford, J. A., Running, S. W., & Frissell, C. A. (2006). Multiscale geomorphic drivers of groundwater flow paths: subsurface hydrologic dynamics and hyporheic habitat diversity. Journal of the North American Benthological Society, 25(2), 288-303.

Poole, G. C., O'Daniel, S. J., Jones, K. L., Woessner, W. W., Bernhardt, E. S., Helton, A. M., & Beechie, T. J. (2008). Hydrologic spiralling: the role of multiple interactive flow paths in stream ecosystems. River Research and Applications, 24(7), 1018-1031.

Puckett, L. J., Zamora, C., Essaid, H., Wilson, J. T., Johnson, H. M., Brayton, M. J., & Vogel, J. R. (2008). Transport and fate of nitrate at the ground-water/surface-water interface. Journal of environmental quality, 37(3), 1034-1050.

Raymond, P.A., C.J. Zappa, D. Butman, T.L Bott,., J. Potter, P. Mulholland, A.E. Laursen,, W.H. McDowell, D. Newbold (2012), Scaling the gas transfer velocity and hydraulic geometry in streams and small rivers. Limnology and Oceanography: Fluids and Environments, 2, 10.1215/21573689-1597669.

Rice, K. C., & Hornberger, G. M. (1998). Comparison of hydrochemical tracers to estimate source contributions to peak flow in a small, forested, headwater catchment. Water Resources Research, 34(7), 1755-1766.

Salehin, M., Packman, A. I., & Wörman, A. (2003). Comparison of transient storage in vegetated

and unvegetated reaches of a small agricultural stream in Sweden: seasonal variation and anthropogenic manipulation. Advances in Water Resources, 26(9), 951-964.

Schilling, K. E., Zhang, Y. K., & Drobney, P. (2004). Water table fluctuations near an incised stream, Walnut Creek, Iowa. Journal of Hydrology, 286(1), 236-248.

Schilling, K. E., Li, Z., & Zhang, Y. K. (2006). Groundwater–surface water interaction in the riparian zone of an incised channel, Walnut Creek, Iowa. Journal of Hydrology, 327(1), 140-150

Schwartz, F. W., & Zhang, H. (2003). *Fundamentals of ground water*. New York: Wiley.

Sheets, R. A., Darner, R. A., & Whitteberry, B. L. (2002). Lag times of bank filtration at a well field, Cincinnati, Ohio, USA. Journal of Hydrology, 266(3), 162-174.

Stanford, J.A., J.V. Ward (1993), An ecosystem perspective of alluvial rivers: connectivity and the hyporheic corridor, J. N. Am. Benthol. Soc., 12(1), 48-60.

Stonedahl, S. H., Harvey, J. W., Wörman, A., Salehin, M., & Packman, A. I. (2010). A multiscale model for integrating hyporheic exchange from ripples to meanders. *Water Resources Research*, *46*(12).

Todd, D. K. (1956). Ground-water flow in relation to a flooding stream. In Proceedings of the American Society of Civil Engineers (Vol. 81, No. 2, pp. 1-20). ASCE.

Tonina, D. and Buffington, J. M. (2009), Hyporheic Exchange in Mountain Rivers I: Mechanics and Environmental Effects. Geography Compass, 3: 1063–1086. doi: 10.1111/j.1749-8198.2009.00226

Tonina, D., & Buffington, J. M. (2011). Effects of stream discharge, alluvial depth and bar amplitude on hyporheic flow in pool- riffle channels. Water resources research, 47(8).

Tonina, D., de Barros, F. P., Marzadri, A., & Bellin, A. (2016). Does streambed heterogeneity matter for hyporheic residence time distribution in sand-bedded streams?. Advances in Water Resources, 96, 120-126.

Valett, H. M., Dahm, C. N., Campana, M. E., Morrice, J. A., Baker, M. A., & Fellows, C. S. (1997). Hydrologic influences on groundwater-surface water ecotones: heterogeneity in nutrient composition and retention. *Journal of the North American Benthological Society*, *16*(1), 239-247.

Ward, A. S., Schmadel, N. M., Wondzell, S. M., Harman, C., Gooseff, M. N., & Singha, K. (2016). Hydrogeomorphic controls on hyporheic and riparian transport in two headwater mountain streams during base flow recession. *Water Resources Research*.

Walters et al (2003) Geomorphology and Fish Assemblages in a Piedmont River Basin, USA,

Freshwater Biology 48(11):1950-1970 · November 2003

Wett, B., Jarosch, H., & Ingerle, K. (2002). Flood induced infiltration affecting a bank filtrate well at the River Enns, Austria. Journal of Hydrology, 266(3), 222-234.

Whiting, P. J., & Pomeranets, M. (1997). A numerical study of bank storage and its contribution to streamflow. Journal of Hydrology, 202(1), 121-136

Woessner, W. W. (2000). Stream and fluvial plain ground water interactions: Rescaling hydrogeologic thought. Ground Water, 38(3), 423-429. Retrieved from https://search-proquest-com.weblib.lib.umt.edu:2443/docview/236849306?accountid=14593

Wondzell S.M. (2006), Effect of morphology and discharge on hyporheic exchange flows in two small streams in the Cascade Mountains of Oregon, USA, Hydrol. Process., 20:267-287 doi:10.1002/hyp.5902.

Wolman, M. G. (1954). A method of sampling coarse river- bed material. EOS, Transactions American Geophysical Union, 35(6), 951-956.

Appendix A: Tables and Figures

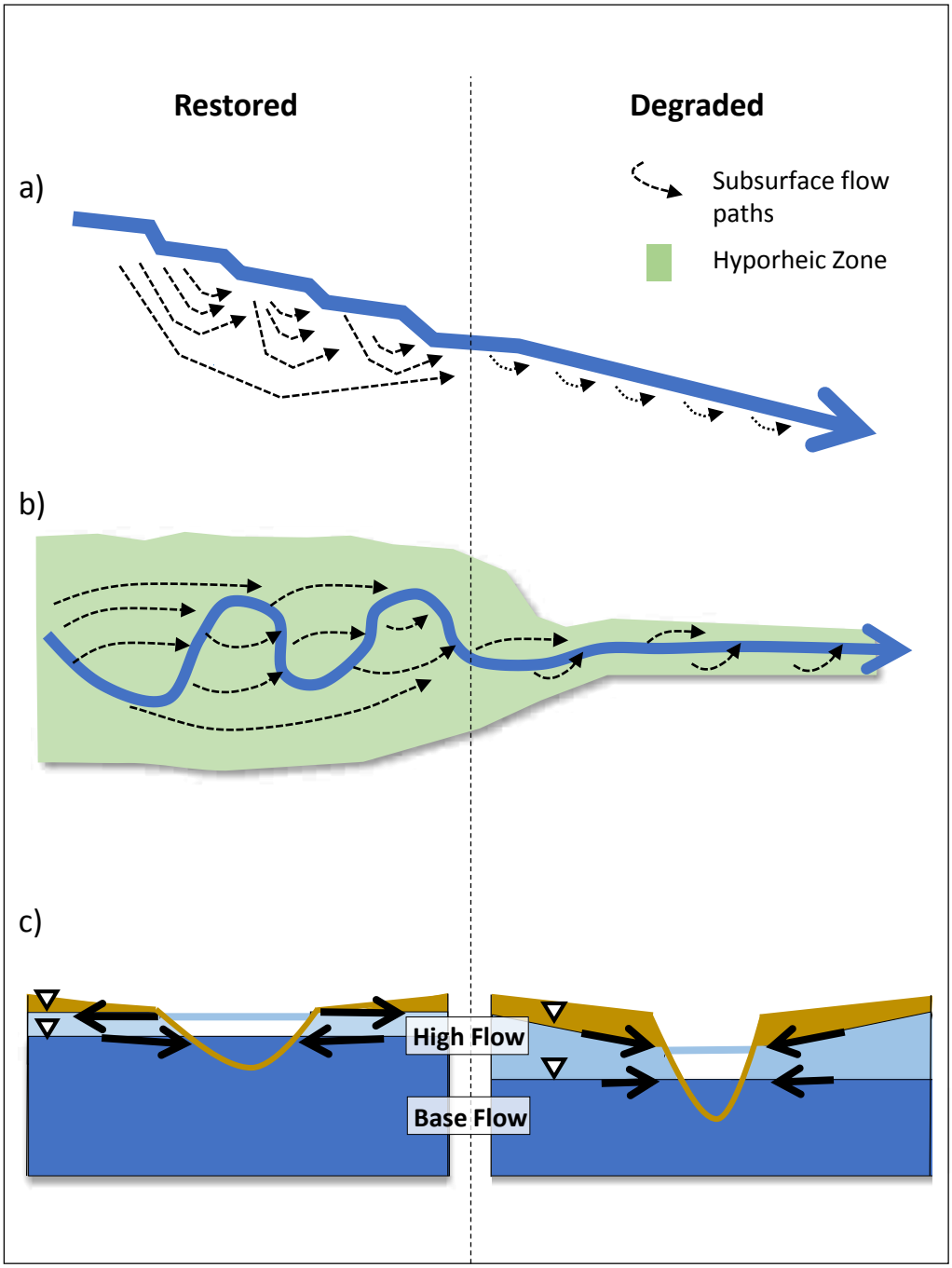

Figure 1: Conceptual model of restoration impacts on exchange. Adding geomorphic complexity in the **(a)** longitudinal and **(b)** planform profiles results in longer, more variable flow paths and a larger hyporheic zone. **(c)** Raising the channel bed elevation increases water table height and prolongs the bank storage period at high flows (light blue) contributing to alluvial aquifer recharge. This results in higher volumetric storage and discharge at base flow (dark blue) .

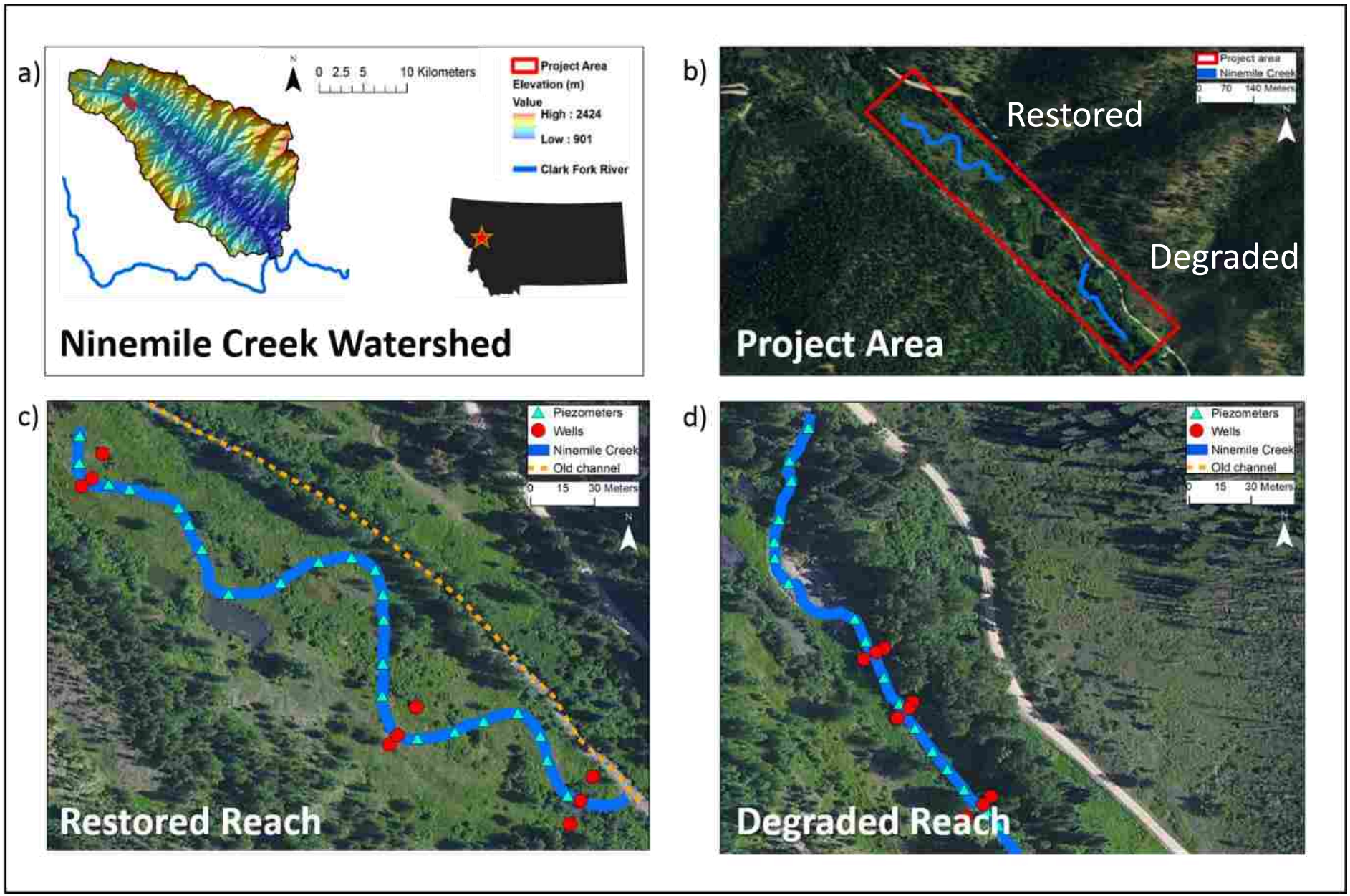

Figure 2. Site map **a)** Regional location of the Ninemile Creek project site **b)** Relative locations of restored and degraded reaches **c-d)** Restored and degraded reaches with piezometers (blue tringles) wells (red circles). The restored reach map also denotes the location of the pre-restoration channel (orange dashed line, not evaluated in this study). Flow direction is to the southeast.

Table 1. Radon model parameter values and methods of estimation.

Parameter		Units	Values		Method for Parameter Estimation
Stream discharge	Q	[m^3 day^{-1}]	12,874 - 57,542		Field measurement (synoptic flow gauging). Mean of upstream and downstream measurements.
^{222}Rn concentration in stream	c	[Bq m^{-3}]	Restored 150 - 663	Degraded 146 - 383	Field sample collection. Analyzed using the RAD7. Varies inversely with Q.
Distance downstream	x	[m]	Restored 351	Degraded 224	Field measurement
^{222}Rn concentration in groundwater (Equilibrium radon concentration)	c_i	[Bq m^{-3}]	26,250		Based on the highest measured seep/shallow well radon concentration. All water samples were analyzed using the RAD7.
Stream width	w	[m]	Restored 7.0	Degraded 5.5	Mean of field measurements.
Evaporation rate	E	[m day^{-1}]	0		Assumed to be negligible (Cook et al., 2006)
Gas transfer velocity across water surface	k	[m day^{-1}]	5.5 - 21.6	6.0 - 27.7	See Table 2
Stream depth	d	[m]	Restored 0.28 - 0.45	Degraded 0.15 - 0.35	Mean of field measurements. Increases with Q.
Decay constant	λ	[d^{-1}]	0.18		Constant
Production in HZ	γ	[Bq m^{-3} day^{-1}]	4,725		$\gamma = \lambda \times c_i$ (from Bourke et al., 2014) where c_i=26,250 Bq/m^3 (highest measured concentration)
Depth of HZ	h	[m]	1		Radon concentrations at 0.5m depth were consistently lower than secular equilibrium values, inferring that hyporheic exchange is present at this depth.
Porosity of HZ	θ	[--]	0.3		Estimated based on subsurface texture.
Mean residence time in HZ	t_h	[day]	0.25	0.4	$t_h = \frac{c - c_h}{\lambda c_h - \gamma}$ From Bourke et al. (2014) where c_h is the average radon concentration within the hyporheic zone.

Table 2. Equations used to estimate gas transfer velocity (k) for radon modeling based on field measurements of velocity (V), slope (S), depth (D) and temperature (included in k_{600} calculation of Raymond et al., 2012 equations)

Equation Citation	Equation
Raymond et al. (2012)	$k_{600} = (VS)^{0.89\pm0.02} \times D^{0.54\pm0.03} \times 5037 \pm 604$
Raymond et al. (2012)	$k_{600} = (VS)^{0.76\pm0.027} \times 951.5 \pm 144$
O'Connor and Dobbins (1958)	$k = 9.301 \times 10^{-3} (\frac{v^{0.5}}{d^{1.5}})$
Negulescu and Rojanski (1969)	$k = 4.87 \times 10^{-4} (\frac{v}{d})^{0.85}$

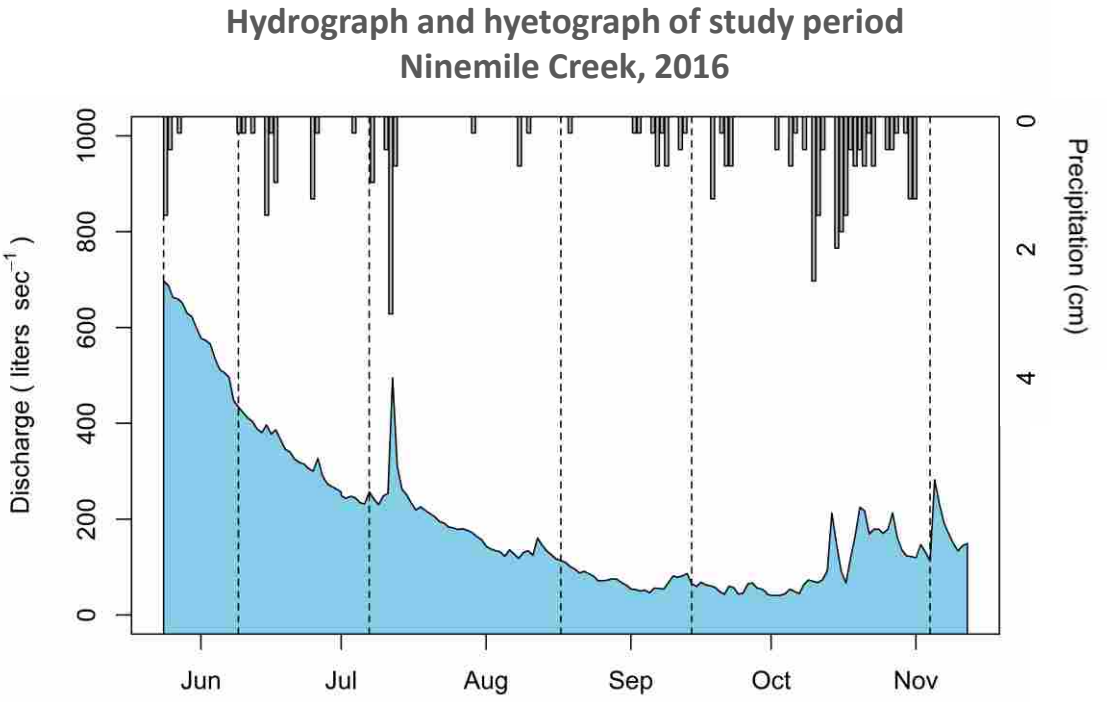

Figure 3. Hydrograph and hyetograph of the study period. Vertical dashed lines represent synoptic sampling dates. The hydrograph was created using a rating curve developed with six dilution gauging discharge measurements from the project site and stream stage measurements from site stilling wells. Precipitation was measured at the Sleeping Woman (#783) SNOTEL site, located 25 kilometers southeast and 600 meters above the study site. Precipitation data are presented to represent the timing, not magnitude, of precipitation at the project site.

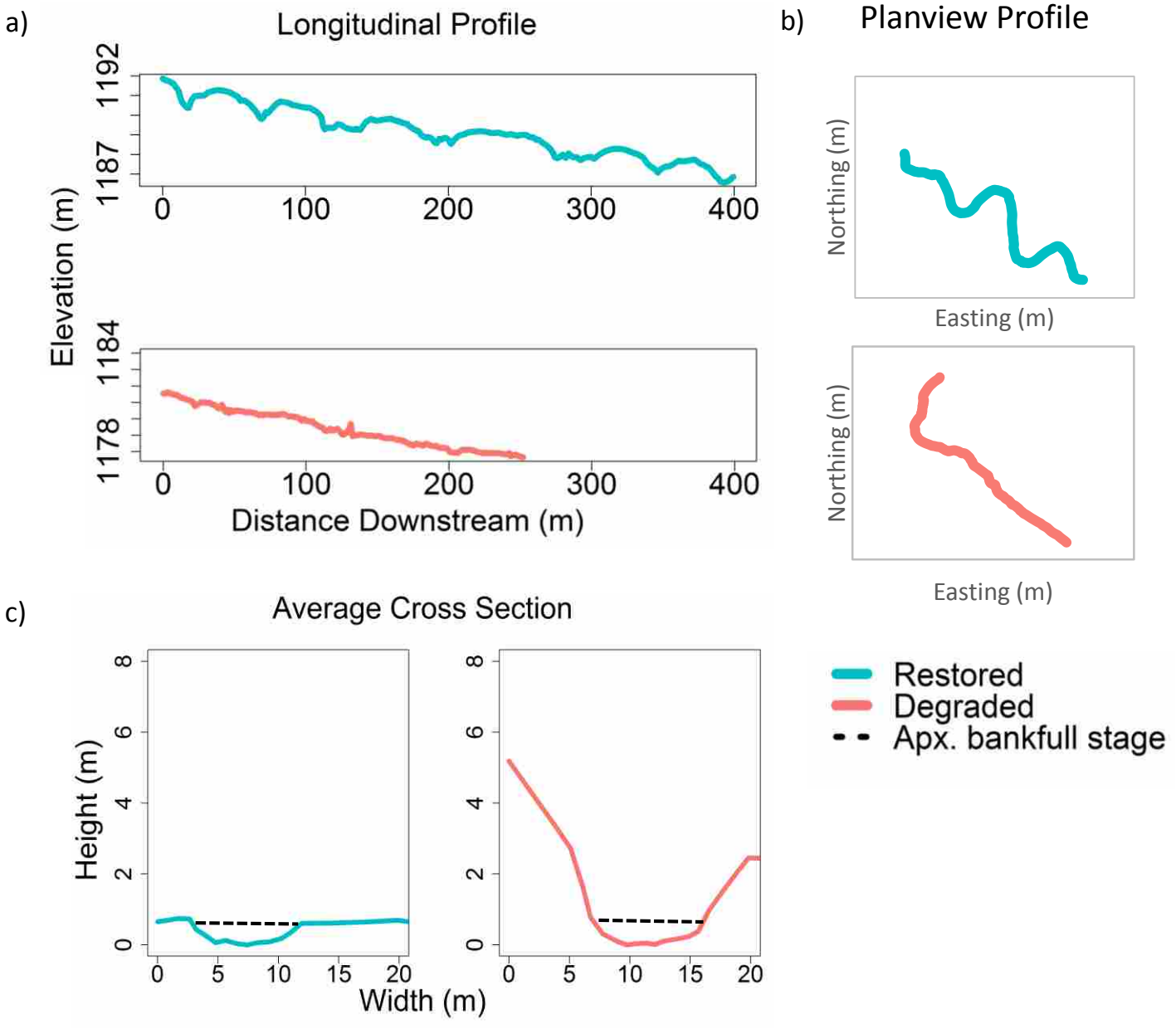

Figure 4. Topographic surveys completed in restored (blue) and degraded (red) reaches **a)** longitudinal profile of bed geometry with points collected at apx. 1-meter resolution along the thalweg **b)** sinuosity with points taken at apx. 1-meter resolution along the thalweg **c)** average channel cross-section with approximate bankfull stage (dashed line).

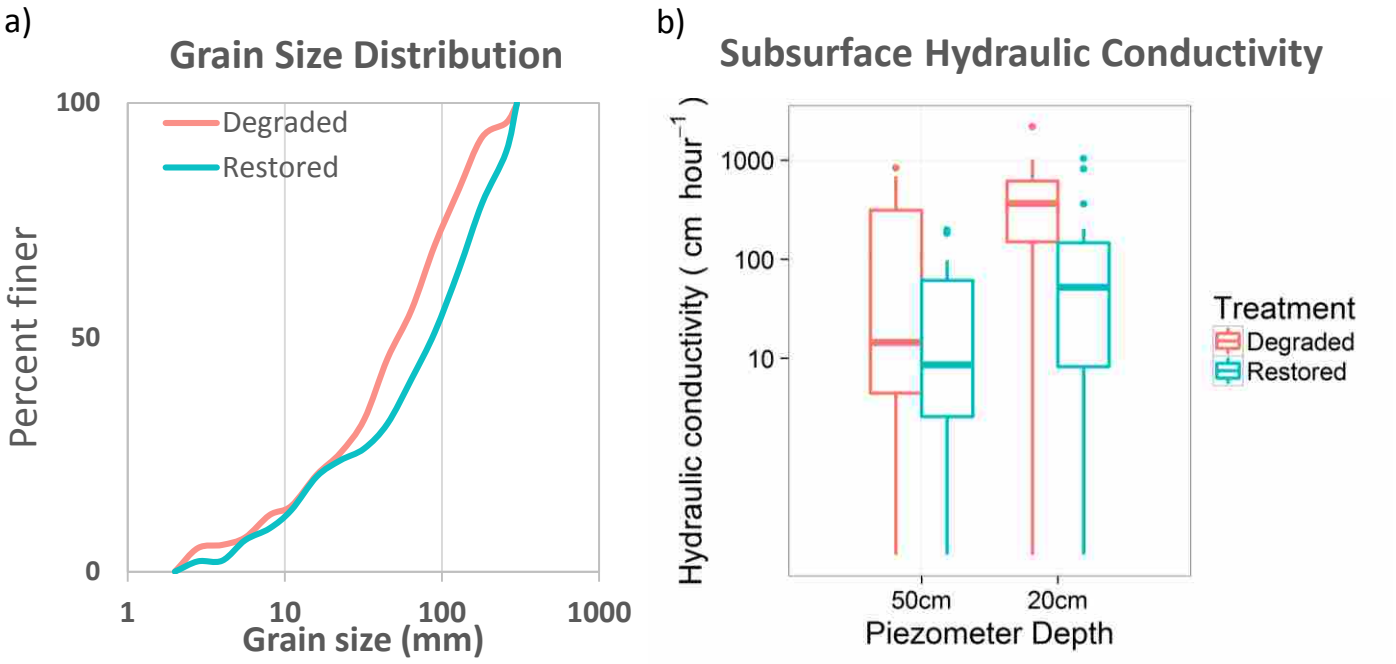

Figure 5 a) Surface grain size distribution measured using Wolman pebble count methods in restored (red) and degraded (blue) reaches **b)** Boxplot of subsurface hydraulic conductivity using Horslev Slug Test Analysis in deep (50cm) and shallow (20 cm) piezometers (n=41 at each depth). Boxplots present median values (line), interquartile range (box) and 1.5x the IQR (whiskers).

Table 3. Summary of topographic and geomorphic surveys

a) Topographic survey results. All metrics are unitless

	Restored	Degraded
Average Width-to-Depth Ratio	18	12
Stream Slope	0.010	0.015
Sinuosity	1.33	1.05
Thalweg variation: r^2	0.927	0.978
Thalweg variation: SD of residuals	32.4	10.3

b) Summary of Subsurface hydraulic conductivities (units are cm hr^{-1})

	Restored		Degraded	
	50 cm	**20 cm**	**50 cm**	**20 cm**
Median	8.6	52.2	14.5	367.6
Upper Quartile	61.3	146.5	312.7	613.8
Lower Quartile	2.6	8.9	4.5	150.2
IQR	58.7	137.6	308.2	462.8

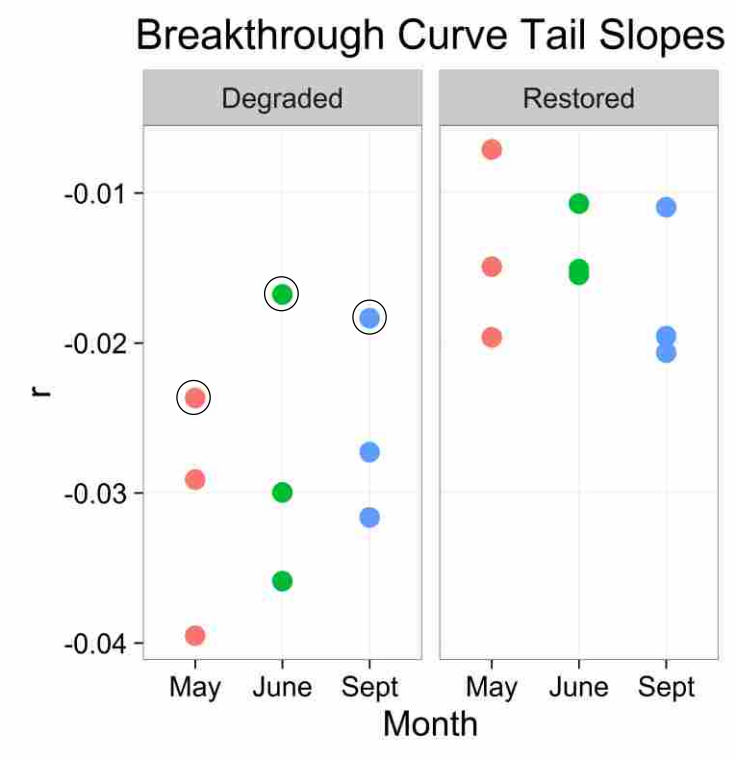

Figure 6. Transient storage as evaluated by *r*, the decay coefficient of BTC tails. Three sub-reaches were evaluated at high (May), moderate (June) and low (September) flows in restored and degraded reaches. An *r*-value closer to zero represents higher transient storage (lower BTC tail slope). The degraded subreach influenced by a channel-spanning beaver dam is circled in black.

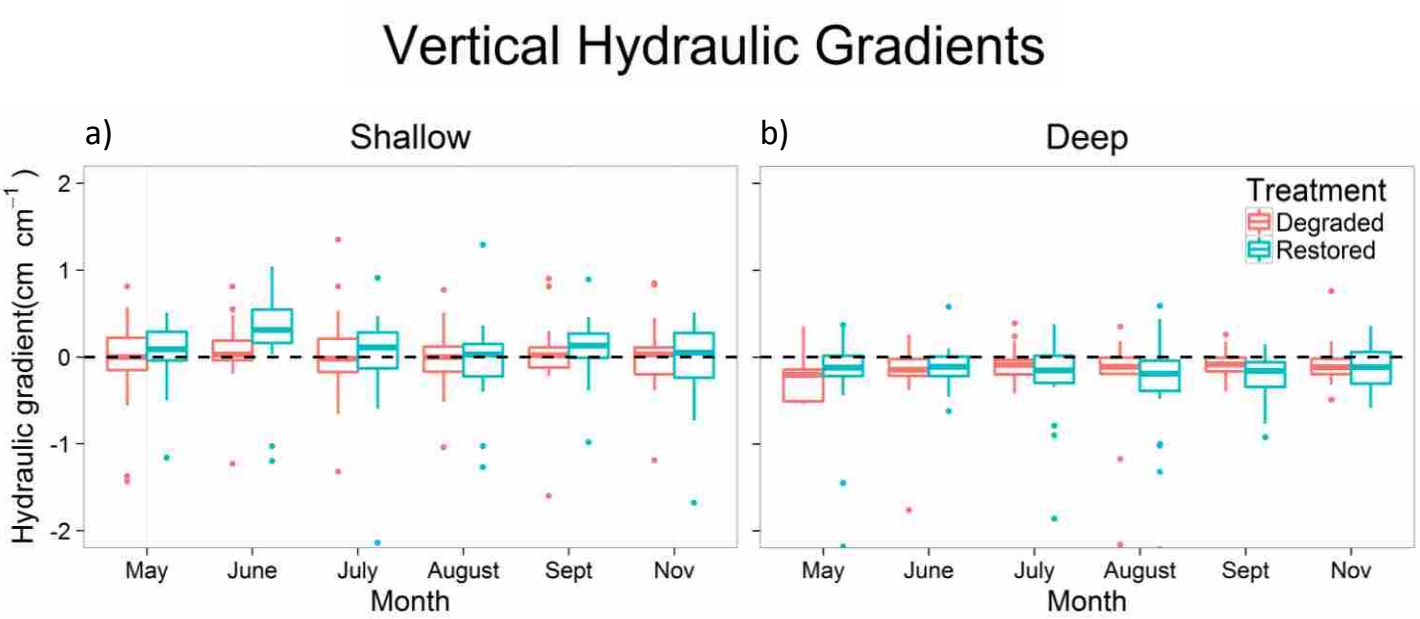

Figure 7. Boxplots of vertical hydraulic gradients calculated from in-stream piezometers in restored (blue) and degraded (red) reaches (at each depth, n=18 in degraded, n=23 in restored). Gradients were calculated at two depths: **a)** between 20 cm subsurface and the streambed (shallow) **b)** between 50 cm and 20 cm subsurface (deep). Positive gradients represent upwelling, negative gradients represent downwelling. Boxplots present median values (line), interquartile range (box) and 1.5x the IQR (whiskers).

Table 4. R^2 values of significant relationships between shallow vertical hydraulic gradient and local bed slope at different length scales in the restored reach. Slope was calculated as the average slope across a range of distances upstream of the piezometer where the hydraulic gradient was measured. The variable length scale accounts for the variable length of bed features and was calculated as the average slope between two sequential piezometers. All significant relationships evaluated are shown, with the best fit (highest r^2) shaded in grey. There were no significant relationships in the degraded reach.

Distance upstream of piezometer (m)	May	June	July	August	Sept-ember	Nov-ember
0.5						0.17
1						0.14
2						
5			0.17		0.13	0.27
7						
9	0.19		0.19			0.15
10	0.17		0.21		0.15	0.17
11			0.17			0.16
13						
Variable	0.20		0.26		0.21	0.19

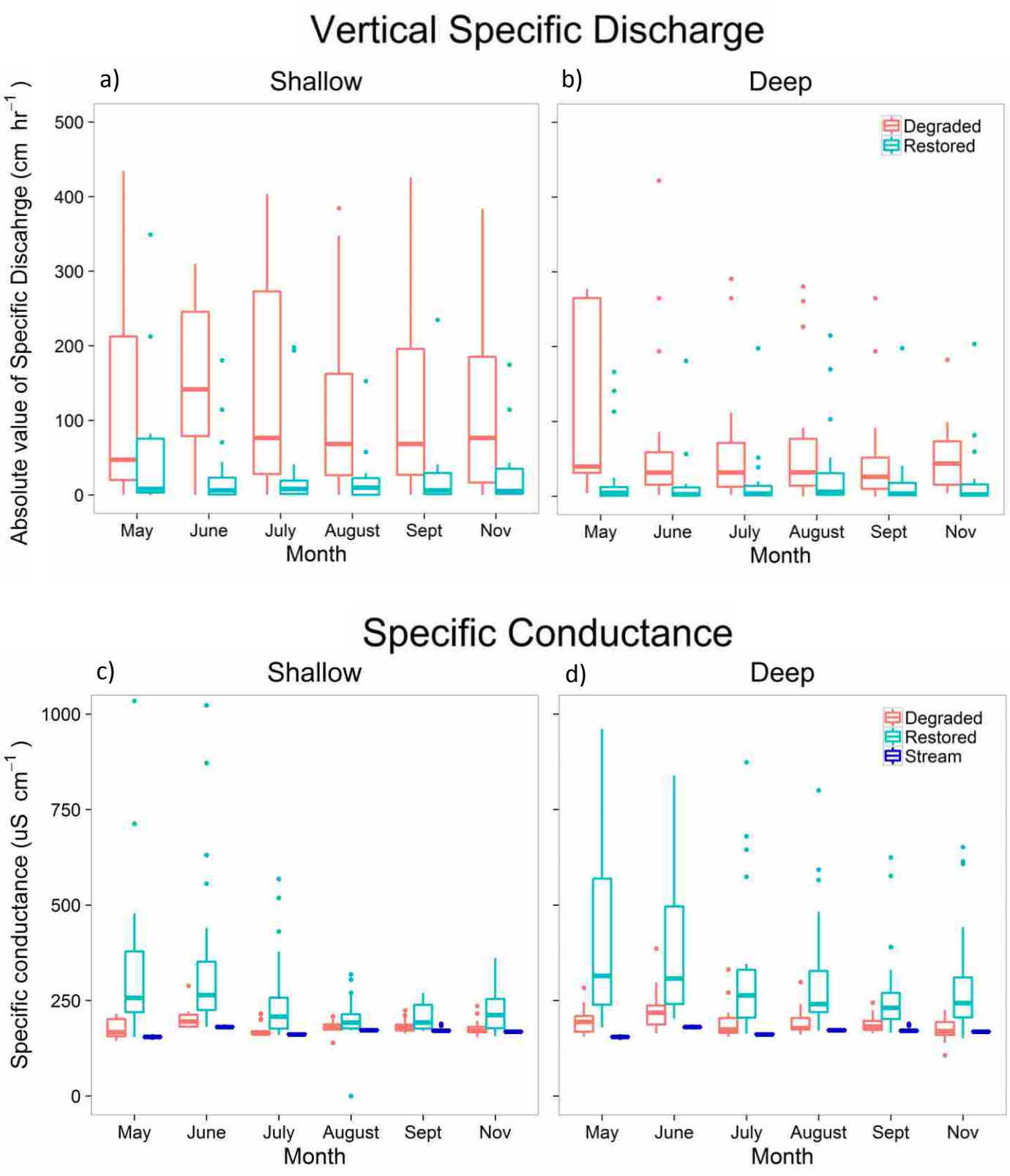

Figure 8. Boxplots of vertical specific discharge and specific conductance from in-stream piezometers at two subsurface depths, (n=18 in degraded, n=23 in restored at each depth). Specific discharge was calculated for flowpaths between **a)** 20 cm subsurface and the streambed **b)** 50 cm – 20 cm subsurface. Absolute values represent the total flux (upwelling and downwelling). See figure 7 for gradients illustrating the direction of flow. SC measurements of water at **c)** 20 cm and **d)** 50 cm subsurface. Boxplots present median values (line), interquartile range (box) and 1.5x the IQR (whiskers).

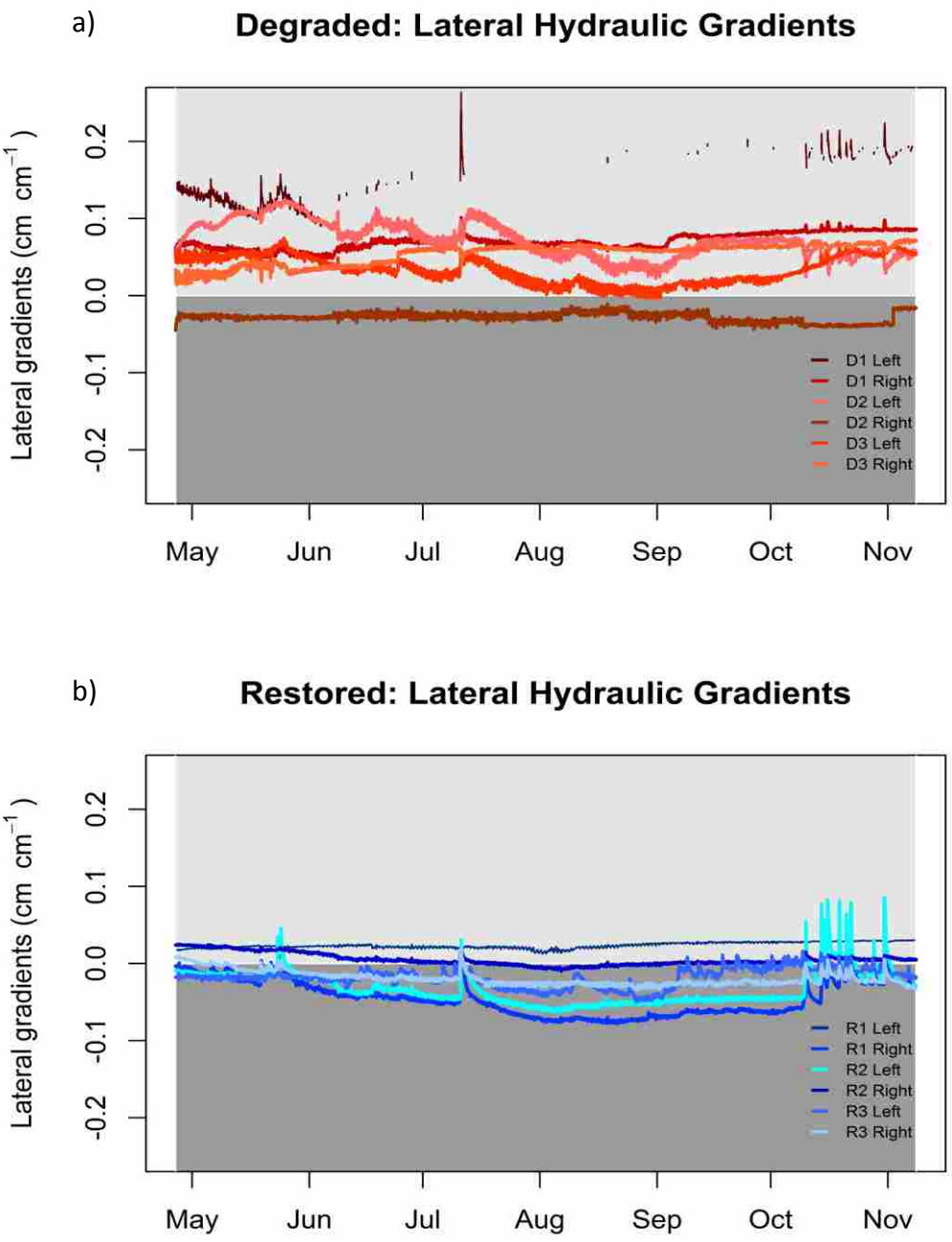

Figure 9. Lateral hydraulic gradients calculated between shallow groundwater wells and in-stream stilling wells in **a)** degraded and **b)** restored reaches. Plots present gradients over time for all wells (n=6 per treatment). Positive gradients represent gains to the stream while negative gradients represent losses. Water levels occasionally dropped below the well extent in degraded reach well D1 left (no line).

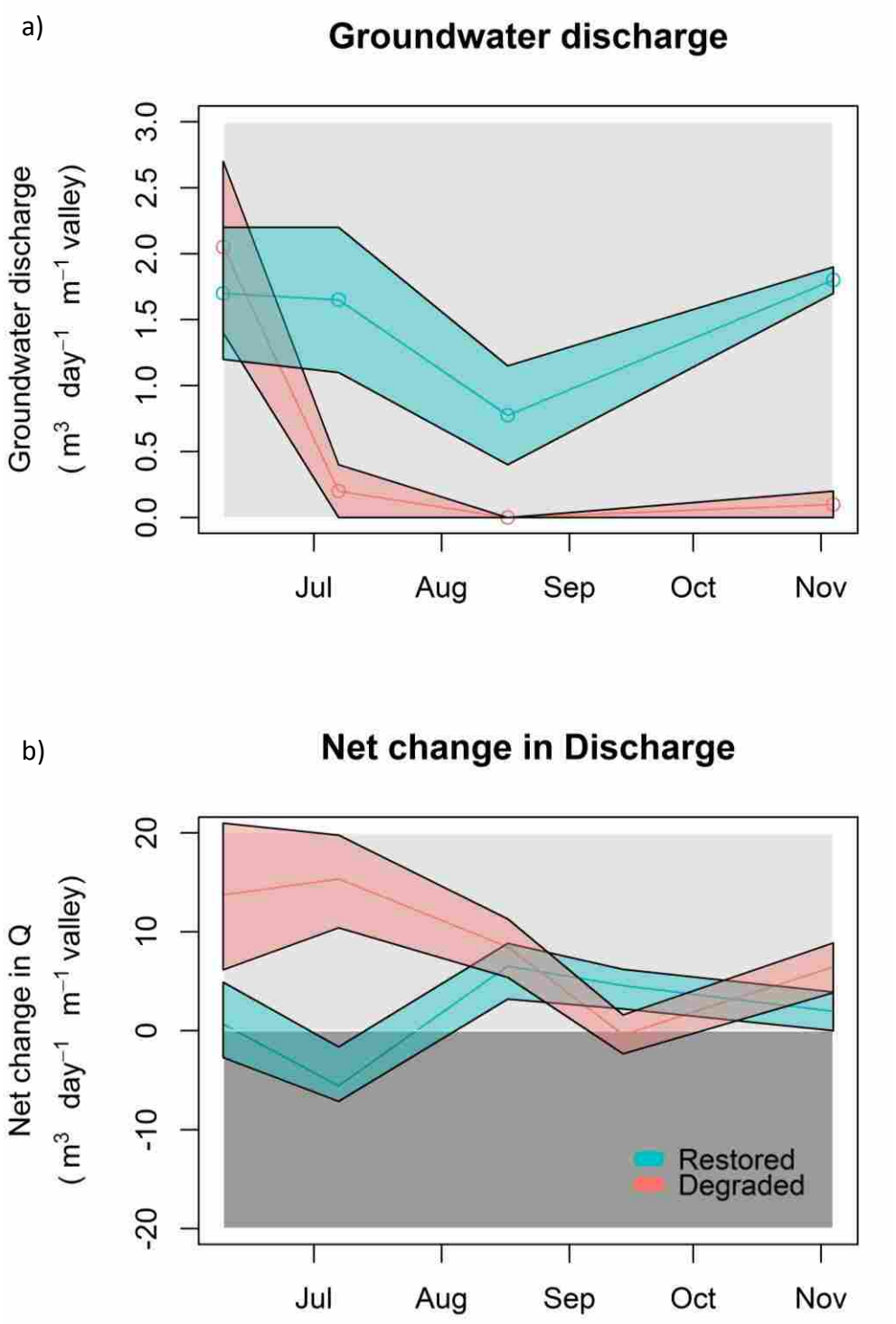

Figure 10. Temporal trends in alluvial aquifer recharge and discharge**. a)** Radon-modeled groundwater discharge over time. Center line represents mean modeled discharge . Shaded areas illustrate model results with +/- 1 standard deviation of radon concentration measurement error. **b)** Net change in discharge over time. Positive values represent a net gaining reach and negative values net losing. Shaded areas represent discharge measurement error. All measurements are normalized by valley length to represent the valley-scale impact of restoration.